國立交通大學

電子物理研究所

碩士論文

奈米圖形二維電子系統 Z_2 拓樸性質之穩健性

ROBUSTNESS OF THE Z_2 TOPOLOGICAL PROPERTY OF A NANO-PATTERNED TWO-DIMENSIONAL ELECTRON GAS

研 究 生 ：吳雨柔

指導教授：朱仲夏教授

中 華 民 國 一 百 ◯ 三 年 九 月

奈米圖形二維電子系統 Z_2 拓樸性質之穩健性

ROBUSTNESS OF THE Z_2 TOPOLOGICAL PROPERTY OF A NANO-PATTERNED TWO-DIMENSIONAL ELECTRON GAS

研 究 生：吳雨柔　　Student : Yu-Rou Wu

指導教授：朱仲夏教授　　Advisor : Prof. Chon Saar Chu

國 立 交 通 大 學

電 子 物 理 研 究 所

碩 士 論 文

A Thesis
Submitted to Department of Electrophysics
College of Science
National Chiao Tung University
in Partial Fulfillment of the Requirements
for the degree of
Msster
In
Electrophysics

September 2014
Hsinchu, Taiwan, Republic of China

中華民國一百○三年九月

奈米圖形二維電子系統 Z_2 拓樸性質之穩健性

研究生：吳雨柔　　指導教授：朱仲夏教授

國立交通大學
電子物理研究所

摘要

二維電子氣在奈米圖樣化的三角晶格位能中，低能量帶可發現相對論性零質量狄拉克費米子。另一方面，自旋軌道作用會在狄拉克點打開能隙並將類金屬轉換成 Z_2 拓樸絕緣體。

根據這些現象，我們更進一步探討 Z_2 拓樸性質在外加磁場下的穩健性。使用 $\mathbf{k}\cdot\mathbf{p}$ 理論寫下在磁場中低能量帶之等效 Hamiltonian 並解析上地計算能帶的 Chern 值。當只有平行平面方向磁場出現時，沿著垂直平面方向的向上自旋態與向下自旋態將被平行磁場耦合，而不再是良好的量子態。這些被混合的自旋態將破壞系統原本的 Z_2 拓樸特性；如果再加上一個垂直平面方向的微小磁場，系統將可以回復 Z_2 拓樸特性，這意味著 Z_2 拓樸性質在適當外加磁場下的穩健性。

Robustness of the Z_2 Topological Property of a Nano-patterned Two-dimensional Electrons Gas

Student: Yu-Rou Wu Advisor: Prof. Chon-Saar Chu

Department of Electrophysics
National Chiao Tung University

Abstract

The relativistic massless Dirac fermions is found in the low energy bands of the two-dimensional electron gas subjected to triangular nano-patterned periodic potential. The spin-orbit interaction further introduces gap at Dirac points for the massless fermions and turns the semimetal into a Z_2 topological insulator.

Base on these facts, we investigate the robustness of the Z_2 topological nature of the system under external magnetic field. The $\mathbf{k}\cdot\mathbf{p}$ theory is employed to develop the effective Hamiltonian for the low energy bands with the presence of magnetic field. We analytically calculate the Chern numbers of the bands. For the presence of only in-plane magnetic field, the up and down spin along out-of-plane direction are no more good quantum states. The mixing of these states ruins the Z_2 feature of the system. However, with arbitrary small out-of-plane magnetic field, the Z_2 topological nature is restored meaning the robustness of its topology under external magnetic field.

致謝

感謝朱老師在我碩班生活中耐心的指導，縝密的邏輯思考，謹慎細心地研究方式，使我收穫良多。並感謝實驗室的學長姐們的建議與幫忙，同學徐豪與學弟們的陪伴與協助。謝謝關心我的家人，還有交大的資源與人力使我能完成碩士學位，一切一切，十分感激。

Contents

List of Figures

(isotropic band structures, independent of α) is accurate. The parameters we employ here are $m^* = 0.023m_e$; the MTP strength $U_0 = 165$ meV with diameter $d = 0.663a$, and $a = 40$ nm is the lattice constant. The SOI coupling constant is $\lambda = 120\text{Å}^2$

3.1 The lowest four bands of 2DEG subjected to MTP lattice. The blue solid lines (double degenerate) are those with $\mathbf{B}_\parallel = 0$T, while the red solid lines are those with $\mathbf{B}_\parallel = 3$T. The SOI is present for both of them. For comparison, the band structures without SOI but with $\mathbf{B}_\parallel = 0$T (black dotted lines) and $\mathbf{B}_\parallel = 3$T (gray dashed lines) are also shown. The other parameters we employ here are λ =120 Å^2 (InAs); $m^* = 0.023m_e$; $U_0 = 165$meV; $a = 40$nm; $d = 0.663a$.

3.2 The lowest four bands around *K* point of 2DEG subjected to MTP lattice. The blue lines are those with $\mathbf{B}_\perp = 0$T while the red lines are those with $\mathbf{B}_\perp = 0.03$T. The in-plane magnetic field is $\mathbf{B}_\parallel = 3$T for both of them. The other parameters we use here are λ =120 Å^2 (InAs); $m^* = 0.023m_e$; $U_0 = 165$meV; $a = 40$nm; $d = 0.663a$.

3.3 The band structures from the effective theory around *K* point. (a) The out-of-plane field, $\mathbf{B}_\perp = 0$T and (b) $\mathbf{B}_\perp = 0.03$T. The solid red and blue lines are those bands from numerical results with different **q**-directions ($\alpha = 0$ and $\alpha = 10$ for blue and red lines, respectively). The parameters we employ here are $m^* = 0.023m_e$; the MTP strength $U_0 = 165$meV with diameter $d = 0.663a$ and $a = 40$ nm is the lattice constant. The SOI coupling constant is $\lambda = 120\text{Å}^2$

4.1 The Chern numbers of the lowest 4 bands near the *K* point. (a) $\mathbf{B}_\parallel \neq 0, \mathbf{B}_\perp = 0$ (b) $\mathbf{B}_\parallel \neq 0, \mathbf{B}_\perp = |\mathbf{B}_\perp|\hat{z}$ (c) $\mathbf{B}_\parallel \neq 0, \mathbf{B}_\perp = -|\mathbf{B}_\perp|\hat{z}$ (d) $\mathbf{B}_\parallel = 0, \mathbf{B}_\perp = -|\mathbf{B}_\perp|\hat{z}$. The Chern numbers of the band are indicated by the numbers with corresponding color. The SOI are present for all of them. The parameters we employ here are $m^* = 0.023m_e$; the MTP strength $U_0 = 165$meV with diameter, $d = 0.663a$, where $a = 40$ nm is the lattice constant. The SOI coupling constant is $\lambda = 120\text{Å}^2$.

A.1 The top views of the MTP lattice with the a being the distance between the centers of two adjacent disks. The potential is U_0 inside the disk with diameter d and zero outside.

C.1 The energy band structures of 2DEG subjected to MTP lattice. The blue lines are those without SOI while the red lines are those with SOI. The parameters we employ here are $m^* = 0.023m_e$; the MTP strength $U_0 = 165$meV with diameter, $d = 0.663a$, where $a = 40$ nm is the lattice constant. The SOI coupling constant is $\lambda = 120\text{Å}^2$.

C.2 The energy band structures of 2DEG subjected to MTP with SOI and in-plane magnetic field, $\mathbf{B}_\parallel = 3$T. The parameters we employ here are $m^* = 0.023m_e$;

the MTP strength $U_0 = 165\,\text{meV}$ with diameter, $d = 0.663a$, where $a = 40\ \text{nm}$ is the lattice constant. The SOI coupling constant is $\lambda = 120\text{Å}^2$.

D.1 Energy dispersion with in-plane magnetic field at the lowest four bands. At *K* point, there are two degenerate points, indicated by the two black arrows. λ =120 Å^2 (InAs); $m^* = 0.023m_e$; $U_0 = 165\,\text{meV}$; $a = 40\,\text{nm}$; $d = 0.663a$; $B_{\text{in}} =$ 3(Tesla).

List of parameters

K, K'	**Sec.** 1.1	The Dirac points in the reciprocal lattice
$\mathrm{H_{SO}}$	Eq. (1.1)	The Hamiltonian of spin-orbit interaction
$\hbar$	Eq. (1.1)	The plank constant
$\boldsymbol{\sigma}$	Eq. (1.1)	The Pauli matrix
$\mathrm{V}(\mathbf{r})$	**Sec.** 1.3	The external periodic potential, in this thesis it is muffin-tin type potential
$\mathbf{r}$	**Sec.** 1.3	The potential vector of electron
λ	**Sec.** 1.3	The spin-orbit coupling constant
d	**Fig.** 1.2	The diameter of muffin-tin lattice
a	**Fig.** 1.2	The distance of center to center for two nearest neighbor lattice
$\mathrm{U_0}$	**Fig.** 1.2	The strength of muffin-tin potential
$\mathrm{H_0}$	Eq. (2.1)	The Hamiltonian of kinetic term and muffin-tin potential
$\Psi_{\mathbf{k}}(\mathbf{r})$	Eq. (2.1)	The eigen wave-function of $\mathrm{H_0}$
E	Eq. (2.1)	The eigen-energy
$\mathbf{k}$	Eq. (2.1)	The wave vector expanded from K point, is equal to $\mathbf{K}+\mathbf{q}$, $\mathbf{K}$ is the wave vector of K point, $\mathbf{q}$ is a small expansion vector from $\mathbf{K}$, with $\lvert\mathbf{q}\rvert \ll \lvert\mathbf{K}\rvert$
$\mathbf{p}$	Eq. (2.1)	The momentum operator
$\mathbf{G}_n$	Eq. (2.2)	The n-th wave vector of lattice
n, n' …etc	Eq. (2.2) Eq. (2.3)	The band index
m, m'	Eq. (2.4)	The reciprocal lattice index
c_n	Eq. (2.2)	The coefficient of wave-function
$\widetilde{\mathrm{V}}_m$	Eq. (2.3)	The Fourier transform of muffin-tin potential
m^*	**Fig.** 2.1	The effective electron mass
$\mathbf{a_1}, \mathbf{a_2}$	**Fig.** 2.1a	The basis vector of lattice in real space
$\mathbf{b_1}, \mathbf{b_2}$	**Fig.** 2.1b	The basis vector of lattice in reciprocal space
$\mathbf{K_1}$	**Fig.** 2.1b	The vector from the center of Brillouin zone to K point, along the $+x$-direction in $\mathbf{k}$-space
$\boldsymbol{\Gamma}$	**Fig.** 2.2b	The center of the hexagonal Brillouin zone
$\mathbf{M}$	**Fig.** 2.2b	The center between K and K' points

τ	**Sec.** 2.3	The valley index, $+1$ and -1 for K and K' valley, respectively
$\varphi_{\mathbf{k}}(\mathbf{r})$	Eq. (2.12)	The eigen wave-function of $\mathrm{H}_0 + \mathrm{H}_{\mathrm{SO}}$
ε	Eq. (2.12)	The eigen energy for effective Hamiltonian
$\mathrm{H}_{\mathbf{q}}$	Eq. (2.14a)	The perturbed Hamiltonian multiplier from effective theory, $\mathbf{H}_{\mathbf{q}} \cdot \mathbf{q}$ is perturbed Hamiltonian
q_x, q_y	Eq. (2.17)	The $\boldsymbol{x}, \boldsymbol{y}$ components of $\mathbf{q}$
$h_x, h_y,$ $h_1, h_2,$ h_3	Eq. (2.17) Eq. (2.18a) Eq. (2.18b)	The parameters of $\mathbf{H}_{\mathbf{q}}$
h	Eq. (2.21)	The square root of $\boldsymbol{h_x^2 + h_y^2}$
ε_0	**Sec.** 2.3	The eigen energy for the unperturbed Hamiltonian
λ_{SO}	Eq. (2.17)	The matrix elements of $\mathbf{H}_{\mathbf{q}}$ corresponds to spin-orbit interaction strength
$\pi_0,\pi_1,$ π_2,π_3	Eq. (2.18a) Eq. (2.18b)	$\boldsymbol{\pi_0}$ is the $\mathbf{2 \times 2}$ identity and $\{\boldsymbol{\pi_1}, \boldsymbol{\pi_2}, \boldsymbol{\pi_3}\}$ are the Pauli matrices for the space spanned by $\{\|\mathbf{1}, \boldsymbol{\tau}\rangle, \|\mathbf{2}, \boldsymbol{\tau}\rangle\}$
$\sigma_0,\sigma_1,$ σ_2,σ_3	Eq. (2.18a) Eq. (2.18b)	$\boldsymbol{\sigma_0}$ is the $\mathbf{2 \times 2}$ identity and $\{\boldsymbol{\sigma_1}, \boldsymbol{\sigma_2}, \boldsymbol{\sigma_3}\}$ are the Pauli matrices for the spin degrees of freedom
H_{B}	Eq. (3.1)	The Hamiltonian of Zeeman term
$H_{\parallel}$	Eq. (3.1)	The Hamiltonian of in-plane magnetic field
$\mathbf{B}_{\parallel}$	Eq. (3.1)	The in-plane magnetic field
$\mathbf{B}_{\perp}$	Eq. (3.5)	The out-of-plane magnetic field
$H_{\perp}$	**Sec.** 3.3	The Hamiltonian of out-of-plane magnetic field
$\theta_{\mathbf{q}}$	Eq. (3.8)	The angle between $\boldsymbol{q_x}$ and $\boldsymbol{q_y}$
χ_+, χ_-	Eq. (3.9)	The spin-up and spin-down states along the direction of in-plane magnetic field
$\varepsilon_{\parallel}$	Eq. (3.10)	The strength of in-plane magnetic field
$\varepsilon_{\perp}$	Eq. (3.10)	The strength of out-of-plane magnetic field
$\gamma_{\perp}$	Eq. (3.10)	$\boldsymbol{\gamma_{\perp}} = \pm\mathbf{1}$,indicate the direction of out-of-plane magnetic field
H^{eff}	Eq. (3.10)	The effective Hamiltonian
$\|\psi(\mathbf{q})\rangle$	Eq. (4.8)	The eigen solution of $\boldsymbol{H^{\mathrm{eff}}}$
A, B, C, D	Eq. (4.8)	The coefficients of $\|\boldsymbol{\psi}(\mathbf{q})\rangle$
$F_{n,\tau}(\mathbf{q})$	Eq. (4.12)	The multiplier of the Berry curvature for our system
$\Omega_{n,\tau}(\mathbf{q})$	Eq. (4.13)	The Berry curvature of our system
$C_{\eta\xi}$	Eq. (4.15)	The Chern numbers of our system, $\boldsymbol{\eta, \xi} = \pm\mathbf{1}$

Chapter 1

Introduction

The emergence of graphene, carbon atoms arranging into two dimensional (2D) honeycomb lattice, has aroused much attention. It is not only because of the realization of relativistic dynamics in condensed matter physics, but also due to its abundance topological features as spin-orbit interaction (SOI) is introduced. On the other hand, the Dirac features of band structures can be introduced in artificial lattice as well. The energy dispersion of 2D electron gas (2DEG) subjected to nano-patterned external lattice potential has been shown, both experimentally and theoretically, possessing gapless Dirac like structure. Furthermore, the SOI removes the degeneracy at Dirac point and introduces gap opening. With further topological analysis, the gap reveals, itself, the Z_2 topological nature. Base on the knowledge, we further study the robustness of this topological properties under both in-plane and out-of-plane magnetic field, individually and simultaneously. We employ the $\mathbf{k}\cdot\mathbf{p}$ theory to develop the effective Hamiltonian, and base on this Hamiltonian, the topology of the low energy bands are discussed.

Before proceeding, the rest part of this introduction is set to give a brief review of the concepts of topological insulator and spin-orbit interaction. In **Sec.** 1.1, the term of topological insulator is introduced. Historically, the topological nature of quantum Hall effect indicating by Thouless *et al* [1] unveils the new insulating phase relating to topology. Furthermore, Kane and Mele point out a richer topological feature relating to spin in graphene, the quantum spin Hall effect (QSH). These will all discussed in **Sec.** 1.1. In **Sec.** 1.2, the spin-orbit interaction is introduced. In this section, the enhancement of SOI in semiconductor is discussed. And finally, the motivation of this thesis is presented in **Sec.** 1.3.

1.1 Topological insulator

The evolution in condensed matter physics is often propelled by discoveries of novel materials. In this respect, materials presenting unique quantum-mechanical properties are of special importance. Topological insulators (TIs) are a class of such materials and they are currently leading to the surge of research. They are called ‘‘topological’’

because the wave functions of their electronic states span a Hilbert space that has a nontrivial topology. In crystalline solids the wave vector **k** becomes a good quantum number, the wave function can be regarded as a mapping from the **k**-space to a manifold in the Hilbert space, so the topology becomes relevant to the electronic states in solids. A significant consequence of nontrivial topology in an insulator is that a gapless interface state necessarily appears when the insulator is physically terminated and faces an ordinary insulator (including the vacuum). This is because the nontrivial topology is a noncontinuous characteristic of gapped energy states. As long as the gap remains open, the topology cannot change; that is to say, for the purpose of the topology changing across the interface into a trivial one, at the interface the energy gap must close. Such principle for the necessary appearance of gapless interface states is called bulk-boundary correspondence. Furthermore, the peculiar characteristics of the edge/surface states is an another unique property of TIs. Recently the TI research is focused mostly on time-reversal invariant systems, where the nontrivial topology is protected by time-reversal symmetry (TRS).

In 1980, von Klitzing et al. found the Quantum Hall effect (QHE) in a high-mobility 2D semiconductor under high magnetic field and very low temperature [2]. The quantized Hall resistance has plateaus as a function of the number of electrons. Such a quantization of transport coefficients obviously pointed to a macroscopic quantum phenomenon (made by Laughlin's gauge argument **[3]**). In 1982, it was identified by Thouless, Kohmoto, Nightingale, and den Nijs (TKNN) that QHE is not only quantum mechanical but also topological. They demonstrated that in quantum Hall (QH) system the **k**-space is mapped to a topologically-nontrivial Hilbert space, whose topology can be specified by an integer topological invariant called TKNN invariant ν, and that σ_{xy} is equal to ν times e^2/h [1]. The TKNN invariant is also called Chern number. The QH system belongs to a topological class which breaks TRS. In recent years, an new topological class has been proposed. These new quantum states belong to a class which is TR invariant , and where SOI plays an significant role. The quantum spin Hall (QSH) state is a state of matter proposed to exist in special, 2D semiconductors with SOI. The QSH state of matter is the cousin of the integer QH state, but, unlike the latter, it does not require the application of a large magnetic field. The QSH state does not break TRS. The first proposal for the existence of a QSH state was developed by Kane and Mele [4] who adapted an earlier model for graphene by Haldane **[5]** which exhibits an integer QH effect. The Kane and Mele model is two copies of the Haldane model such that the spin up electron exhibits a chiral integer QH effect while the spin down electron exhibits an anti-chiral integer QH effect. It has been recently proposed [6] and subsequently experimentally realized [7] in mercury (II) telluride

(HgTe) semiconductors. The QSH states have zero Hall conductance but it is associate with the Z_2 [8] topological invariant. A Z_2 TI is known to possess a pair of gapless helical edge states protected by TRS. Similar to the gapless chiral edge states of QH systems, responsible for the quantized Hall conductance, the helical edge states ensure the quantization of spin Hall conductance. The Z_2 classification is analogous to the Chern number classification of the QH effect.

1.2 Spin-orbit interaction (SOI)

Spin-orbit coupling (or SOI: spin-orbit interaction) is a well-known phenomenon which connects a particle's spin with its momentum, significantly affecting the atomic energy spectra. In solid-states system, spin-orbit coupling arises from the electron's motion in the intrinsic electric field of the crystal. This interaction makes symmetry breaking because the coupling strength is related to the velocity measured in the reference frame. Thus SOI arises from realistic quantum mechanics and one can obtain the formula of SOI by taking the non-relativistic limit of the Dirac equation. In vacuum the Hamiltonian of SOI is **[9]**:

$$H_{\mathrm{SO}} = -\frac{e\hbar}{4m_0^2c^2}\boldsymbol{\sigma}\cdot(\mathbf{E}\times\mathbf{p}) = \frac{e\hbar}{4m_0^2c^2}\boldsymbol{\sigma}\cdot(\nabla V\times\mathbf{p}), \qquad (1.1)$$

where m_0 is the free electron mass; $\hbar$ is the Plank constant; c is the speed of light. Eq. (1.1) could be illustrated in the framework of the classical electrodynamics. An electron in reference frame moves with velocity $\mathbf{v}$ under an electric field $\mathbf{E}$, finding a magnetic field: $\mathbf{B} = -\frac{1}{c}(\mathbf{v}\times\mathbf{E}) = \frac{1}{mc}(\mathbf{E}\times\mathbf{p})$. That is, the moving electron experiences an equivalent magnetic in its rest frame that origins from the Lorentz transformation of the electric field. Hence this effective magnetic field couples with the electron spin through the magnetic moment of the electron. This physical picture also holds in semiconductor, when $\mathrm{V}(\mathbf{r})$ can be the periodic potential of the host lattice. In addition, the SOI in semiconductor requires an effective electric field. Such effective electric field can be arose from the build-in crystal field has bulk inversion asymmetric (Dresselhaus SOI, in zinc-blende structure) or structural inversion asymmetry (Rashba SOI, in asymmetric quantum wells or heterostructures).

According to the effective mass approximation, the effect of all the fast-varying atomic potential has been reduced to the effective mass. Slower varying $\mathrm{V}(\mathbf{r})$, with the length scale of varying much greater than the spacing of lattice, is found to contribute to SOI with a much larger SO coupling constant λ. For a central potential $\mathrm{V}(\mathbf{r}) = \mathrm{V}(\mathrm{r})$ in vacuum, the SO coupling is:

$$\frac{-\hbar^2}{4m_0^2c^2}\boldsymbol{\sigma}\cdot(\nabla V\times\mathbf{p}) = \frac{\hbar^2}{4m_0^2c^2}\frac{1}{r}\frac{dV}{dr}\boldsymbol{\sigma}\cdot(\mathbf{r}\times\mathbf{p}) = \frac{\hbar^2}{4m_0^2c^2}\frac{1}{r}\frac{dV}{dr}\frac{\mathbf{L}}{\hbar}\cdot\boldsymbol{\sigma} = -\frac{\lambda_{\mathrm{vac}}}{h}\frac{1}{r}\frac{dV}{dr}\mathbf{L}\cdot\boldsymbol{\sigma}$$

where $\mathbf{L}$ is the orbit angular momentum, $\boldsymbol{\sigma}$ is the Pauli matrices and

$$\lambda_{\text{vac}} = \frac{-\hbar^2}{4m_0^2c^2} \approx -3.72 \times 10^{-6}\text{Å}^2$$

While in the semiconductor, also for a central potential $\mathrm{V}(\mathbf{r}) = V(r)$, the SO coupling is:

$$H_{\text{SO}} = -\frac{\lambda}{h}\frac{1}{r}\frac{dV}{dr}\mathbf{L}\cdot\boldsymbol{\sigma}$$

where $\lambda = \approx \frac{P^2}{3}\left[\frac{1}{E_g^2} - \frac{1}{(E_g+\Delta_0)^2}\right]$

For the two dimensional electron gases (2DEG), the SOI becomes:

$$H_{\text{SO}} = -\frac{\lambda}{h}\frac{1}{r}\frac{dV(\rho)}{d\rho}L_z\sigma_z$$

Here P is the momentum matrix element between $s-$ and $p-$ orbitals, E_g is the energy band gap, and Δ_0 represents the SOI energy split to the split-off band [10,11]. In particular $\lambda = 120\text{Å}^2$ in InAs, which is seven order of magnitude greater than λ_{vac} [10].

Qualitatively, this large enhancement of SO coupling constant can be explained in the following. With $\lambda_{\text{vac}} \propto \frac{1}{m_0^2c^2} = \frac{1}{m_0}\frac{1}{m_0c^2}$ we can see that

$$\frac{\lambda}{\lambda_{\text{vac}}} \sim \frac{m^*}{m}\frac{m_0c^2}{E_g}$$

For InAs, $\frac{m_0}{m} \sim \frac{1}{0.023}$; $\frac{m_0c^2}{E_g} \sim \frac{0.5\text{MeV}}{0.418\text{eV}}$ leading to

$$\frac{\lambda}{\lambda_{\text{vac}}} \sim 52 \times 10^6$$

Comparing with $\frac{120\text{Å}^2}{3.73\times10^{-6}\text{Å}^2} = 32 \times 10^6$, such hand waving argument has captured the essential physical origin of the great enhancement.

1.3 Motivation

The material graphene exhibits many remarkable mechanism and electron transport properties due to the presence of Dirac points at the corners of the hexagonal Brillouin zone. In the vicinity of these points, the low energy spectrum is conical, the conduction and valence bands linearly intersecting right at Dirac points, exhibiting relativistic dispersion with zero effective mass. Hence, the graphene can be well described by the massless Dirac Hamiltonian. However, consider with topology, the new physics beyond Dirac Hamiltonian is introduced when SOI is taken into account. Superficially, the SOI introduces energy gap, giving a mass to the particles. Nonetheless, Kane and Mele point out the QSH can be realized in graphene with SOI [12]. The emergence of the gap converts graphene from a 2D semimetal to a Z_2 topological insulator which realizes the QSH effect.

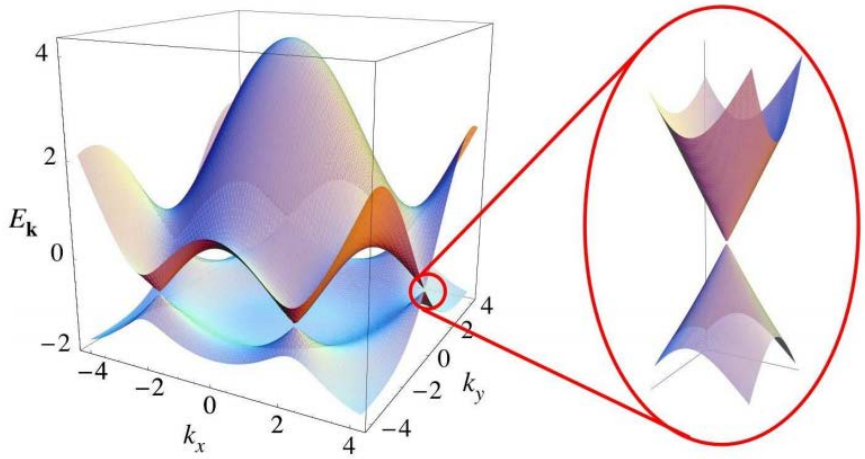

Fig 1.1 : The band structures of graphene with the Dirac points [13].

Beside graphene, the Dirac features of band structures also appear in nano-patterned lattice. C. H. Park and S. G. Louie theoretically proposed that the massless Dirac fermions are found in 2DEG under a triangular muffin-tin potential (MTP) lattice shown in **Fig** 1.2. [14]. Base on these findings, the former thesis of W. L. Su, from our group, further considers the SOI in MTP and discusses the topological properties of the Dirac fermions. The results, in conclusion, the SOI introduces the gap for the Dirac points and it reveals the Z_2 TI nature. **Fig** 1.3 shows the band structures and the corresponding Chern numbers which summarizes the work of W. L. Su [15].

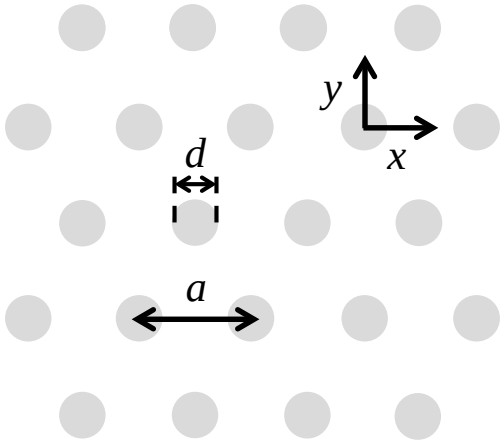

Fig 1.2 : The top view of the MTP lattice with center to center distance a. The potential is U_0 inside the disk with diameter d and zero outside.

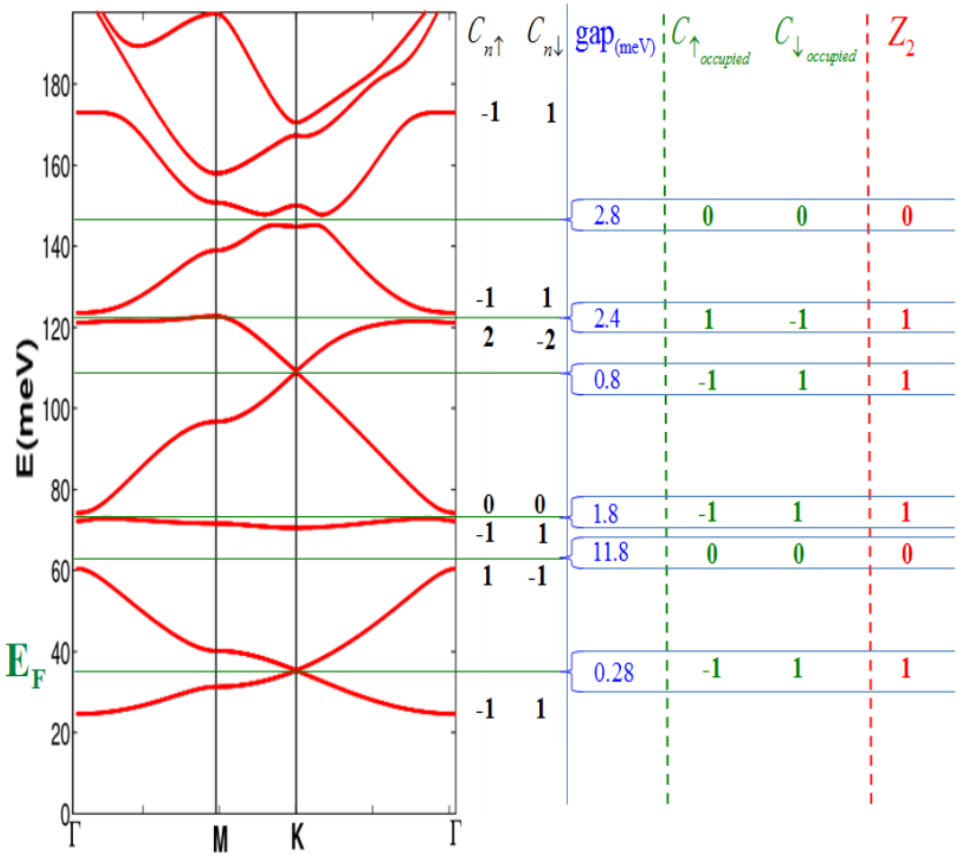

Fig 1.3 : This figure is quoted from the thesis by W. L. Su [15]. It shows the Chern numbers of spin-up and spin-down for each energy bands and the comparison for Fermi energy, $C_{\uparrow occupied}$, $C_{\downarrow occupied}$, Z_2 number

On the other hand, the experimental realization of nano-patterned MTP in honeycomb lattice is achieved by M. Gibertini *et al* [16]. It is found that the massless Dirac points, at the corners of Brillouin zone, can be created by modulating 2DEG with long-wavelength periodic potential (modulation-doped GaAs quantum well). **Fig** 1.4 shows the scanning electron micro images of the nano-patterned modulation doped GaAs/AlGaAs and **Fig** 1.5 shows the setup of experiment.

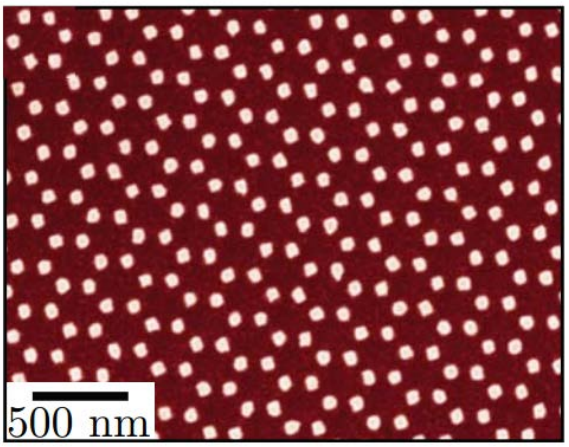

Fig 1.4 : Scanning electron microscopy images of the nano-patterned modulation doped GaAs/AlGaAs sample [16].

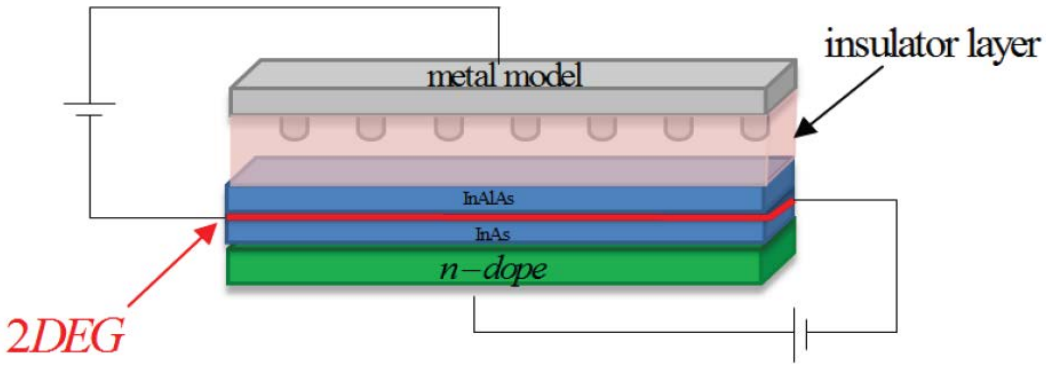

Fig 1.5 : The experimental setup of the 2DEG subjected to MTP lattice. We use the external bias making the n-dope layer to control the Fermi energy.

In this thesis, based on W. L. Su's results [15], we study the robustness of the Z_2 feature under in- and out-of- plane magnetic fields, individually and simultaneously. The energy region we focus on in this thesis is the lowest two energy bands around the

Dirac points (i.e. *K*- and *K'*-valleys). We discuss the robustness of Z_2 topological property under difference cases of magnetic field. We expect that the non-trivial topological properties for nano-patterned 2DEG in MTP could be robustness against the external magnetic fields.

1.4 A guide to this thesis

The goal of this thesis is to investigate the robustness of the Z_2 topological feature of 2DEG in MTP lattice with SOI in the presence magnetic field. The energy dispersion without magnetic field is presented in **Chapter** 2. Besides, the $\mathbf{k}\cdot\mathbf{p}$ theory is employed to develop the effective Hamiltonian for low energy bands. In **Chapter** 3, we discuss the band structures for MTP lattice with SOI and magnetic field. Base on the effective Hamiltonian introducing in **Chapter** 2, the effective theory for the presence of magnetic field is also developed. On top of these, the topological properties of the bands are demonstrated in **Chapter** 4. And finally, the conclusion and future work are shown in **Chapter** 5.

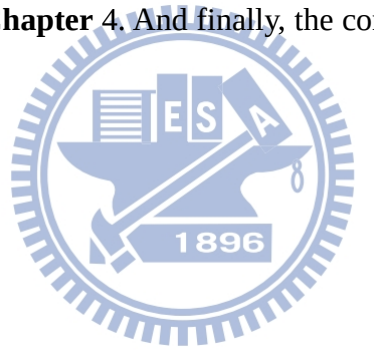

Chapter 2

Energy bands with spin-orbital interaction (SOI)

In this chapter, we discuss the band structures of the two-dimensional electron gas (2DEG) in the presence of the muffin-tin potential (MTP) lattice with (**Sec.** 2.1) and without (**Sec.** 2.2) spin-orbit interaction (SOI). For the low energy band structures, the SOI introduces the energy gap at the *K* and *K'* points, which crucially affects the topological features. Since in the following chapters, we will focus on the band topological properties of the low energy region, in **Sec.** 2.3, we further develop the low energy effective theory around *K* and *K'* points, which is the preparation for the analytically topological discussion.

2.1 Energy bands without SOI

First we start by discussing the energy dispersion of the MTP lattice without SOI. The Schrödinger equation of the 2DEG under the periodic potential is

$$H_0\Psi_{\mathbf{k}}(\mathbf{r}) = \left\{\frac{\mathbf{p}^2}{2m^*} + V(\mathbf{r})\right\}\Psi_{\mathbf{k}}(\mathbf{r}) = E\Psi_{\mathbf{k}}(\mathbf{r}), \tag{2.1}$$

where m^* is the effective electron mass; $V(\mathbf{r})$ is the periodic MTP with $V(\mathbf{r}) = \sum_m \tilde{V}_m e^{i\mathbf{G}_m\cdot\mathbf{r}}$. Due to the periodicity of the Hamiltonian in Eq. (2.1), the solution of the Schrödinger equation is in the Bloch form

$$\Psi_{\kappa}(\mathbf{r}) = \frac{1}{\sqrt{N\cdot A_\Omega}} e^{i\mathbf{k}\cdot\mathbf{r}} \sum_m e^{i\mathbf{G}_m\cdot\mathbf{r}} c_m \tag{2.2}$$

where N is the number of unit is cell and A_Ω is the area of unit cell in real space. The m (and n) labels the reciprocal lattice points, $\mathbf{G}$. The Fourier transform of the MTP (derived in **Appendix A**) is

$$\tilde{V}_m = \frac{2\pi U_0 d}{\sqrt{2}|\mathbf{G}_m| a_1 a_2} J_1\left(\frac{|\mathbf{G}_m| d}{2}\right). \tag{2.3}$$

Substitute Eqs. (2.2), and (2.3) into Eq. (2.1),

$$\sum_n e^{i\mathbf{k}\cdot\mathbf{r}} e^{i\mathbf{G}_n\cdot\mathbf{r}} \left[\frac{\hbar}{2m^*}|\mathbf{k}+\mathbf{G}_{m'}|^2\right] c_{m'} + \sum_{m\,m'} e^{i\mathbf{k}\cdot\mathbf{r}} e^{i(\mathbf{G}_{m'}+\mathbf{G}_m)\cdot\mathbf{r}} \tilde{V}_m c_{m'} = E\sum_{m'} e^{i\mathbf{k}\cdot\mathbf{r}} e^{i\mathbf{G}_{m'}\cdot\mathbf{r}} c_{m'}. \tag{2.4 a}$$

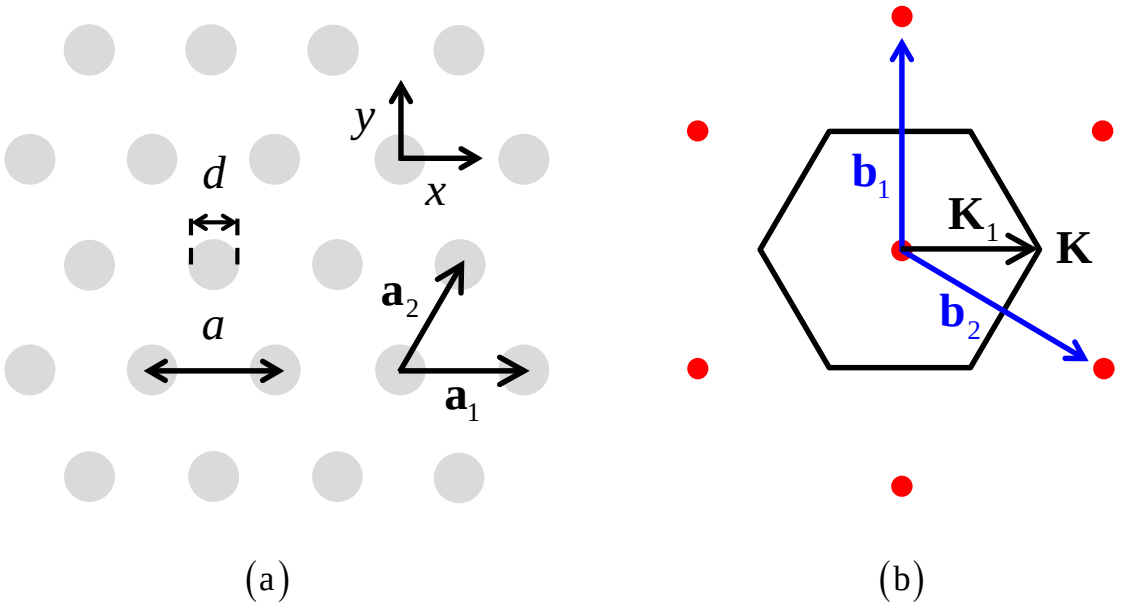

Fig. 2.1 (a) A top view of MTP lattice with distance a between the centers of adjacent potential disks. The potential is U_0 inside the disk with diameter d and zero inside. (b) The reciprocal lattice and the first Brillouin zone.

The second summation in Eq. (2.4) can be further simplified by the index relabeling. Specifically, let $\mathbf{G}_{m''} = \mathbf{G}_{m'} + \mathbf{G}_m$, and $m = m'' - m'$, thus we have

$$\sum_{m\,m'} e^{i\mathbf{k}\cdot\mathbf{r}} e^{i(\mathbf{G}_{m'}+\mathbf{G}_m)\cdot\mathbf{r}} \tilde{V}_m c_{m'} = \sum_{m'\,m''} e^{i\mathbf{k}\cdot\mathbf{r}} e^{i\mathbf{G}_{m''}\cdot\mathbf{r}} \tilde{V}_{m''-m'} c_{m'} = \sum_{m\,m'} e^{i\mathbf{k}\cdot\mathbf{r}} e^{i\mathbf{G}_{m'}\cdot\mathbf{r}} \tilde{V}_{m'-m} c_m \qquad (2.4\text{ b})$$

In the final step in Eq. 2.4(b), the replacements of $n' \to n$ and $n \to m$ are done. After simplification, we arrive

$$\sum_m \left[\frac{\hbar^2}{2m^*} \left|\mathbf{k}+\mathbf{G}_{m'}\right|^2 \delta_{mm'} + \tilde{V}_{m'-m} \right] c_m = E c_{m'} . \qquad (2.5)$$

Let $M_{mm'} = \left[\frac{\hbar^2}{2m^*} \left|\mathbf{k}+\mathbf{G}_{m'}\right|^2 \delta_{mm'} + \tilde{V}_{m'-m} \right]$, and Eq. (2.5) is in the compact matrix form

$$\begin{bmatrix} & M_{mm'} & \end{bmatrix} \begin{bmatrix} c_m \end{bmatrix} = E \begin{bmatrix} c_m \end{bmatrix} \qquad (2.6)$$

The energy band structures in the MTP lattice is shown in Fig. 2.1. Since we are interested in low energy bands, only lowest two bands are presented here. From Fig. 2.1, the bands touch at *K* and *K'* points, at the Brillouin zone corners, result in Dirac cones at these points. The band structures are consistent with the results proposed by C. H. Park and S. G. Louie [14].

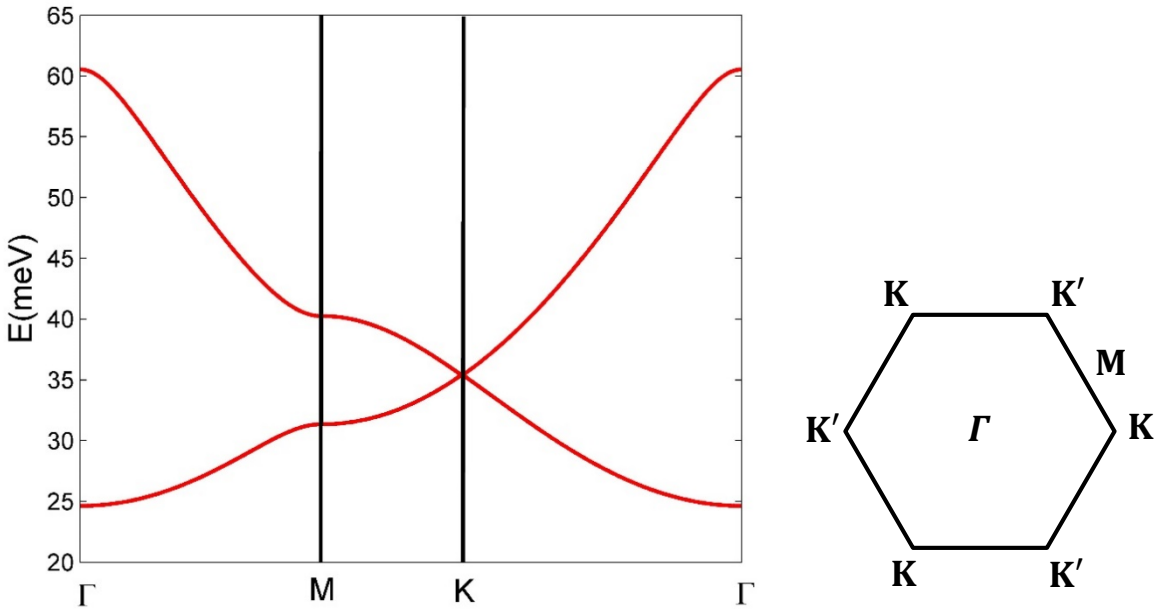

(a) (b)

Fig. 2.2 (a) The lowest two bands of 2DEG subjected to MTP without SOI. The Dirac point is at the touching points (at *K* and *K*' points) of the two bands. For symmetry reasons, the band structures around *K*' point are not shown here. (b) The Brillouin zone with the symmetry points in k-space. The parameters we employ here are $m^* = 0.023m_e$; the MTP strength $U_0 = 165$meV with diameter, $d = 0.663a$, where $a = 40$ nm is the lattice constant.

Since we will derive the $\mathbf{k}\cdot\mathbf{p}$ effective Hamiltonian around Dirac points, the symmetry properties of the degenerated states at *K*- and *K*'- valleys are crucial. Figs. 2.2 and 2.3 show the contours of these states for *K*- and *K*'- valleys, respectively. Specifically, the real and imaginary parts of first band (ψ_1) at *K*-valley are plotted in Fig. 2.2 (a) and (b), while the real and imaginary parts of the second band, ψ_2, are shown in Fig. 2.2 (c) and (d), subsequently. The counterparts of these band states, ψ_1' and ψ_2', at *K*'-valley are in Fig. 2.3. From these figures, we find ψ_1 and ψ_1' are odd functions under mirror reflection with respect to *x* axis ($y \rightarrow$ -*y*), while ψ_2 and ψ_2' are even under the same symmetry operation. These symmetry properties will be employed in the derivation of the $\mathbf{k}\cdot\mathbf{p}$ Hamiltonian in **Sec. 2.4** and the discussion in **Sec. 3.1**.

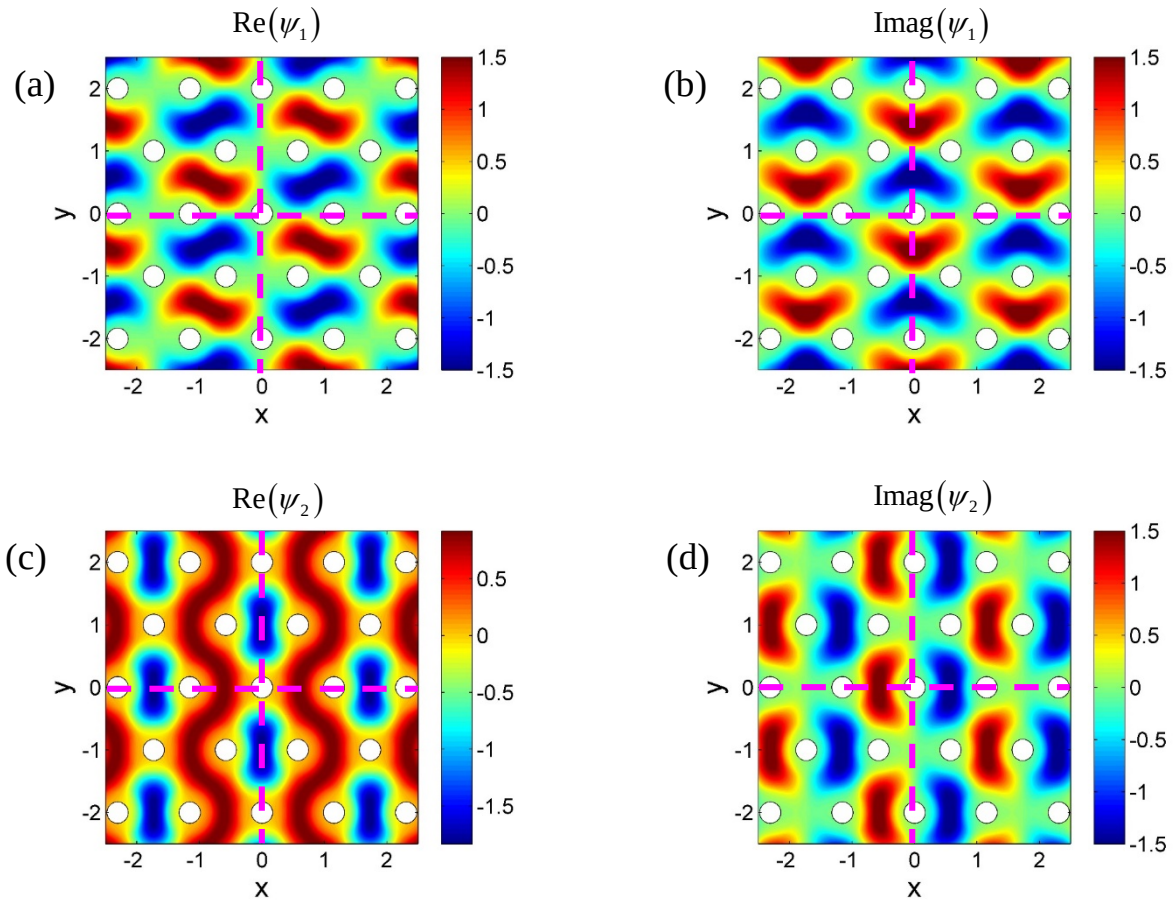

Fig. 2.2 (a) the real part of ψ_1 at *K*-valley (odd under $y \rightarrow -y$). (b) the imaginary part of ψ_1 at *K*-valley (odd under $y \rightarrow -y$). (c) the real part of ψ_2 at *K* valley (even under $y \rightarrow -y$). (d) the imaginary part of ψ_2 *K*-valley (even under $y \rightarrow -y$). The parameters we employ here are $m^* = 0.023m_e$; the MTP strength $U_0 = 165$meV with diameter, $d = 0.663a$, where $a = 40$ nm is the lattice constant.

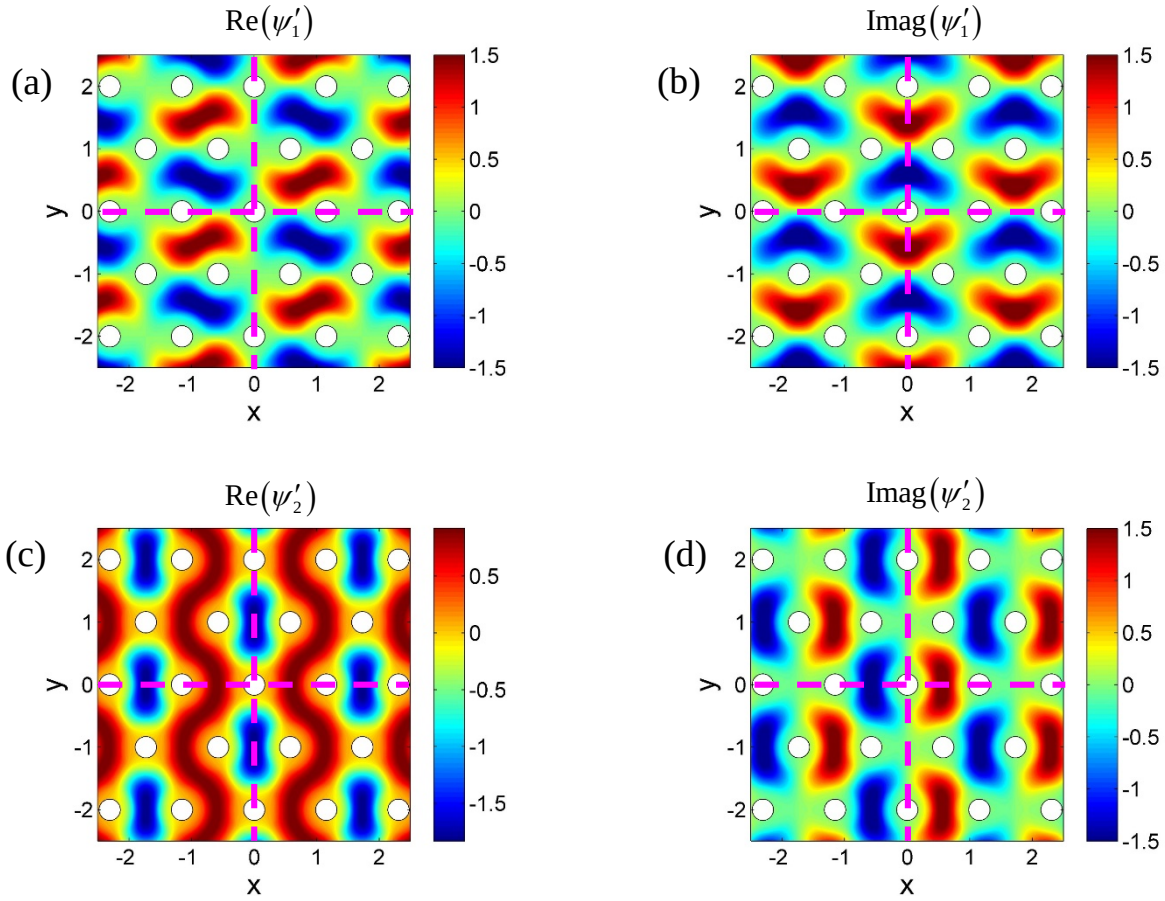

Fig. 2.3 (a) The real part for the 1st band at *K*'-valley (odd under $y \rightarrow -y$). (b) The imaginary part for the 2nd band at *K*'-valley (odd under $y \rightarrow -y$). (c) The real part for the 2nd band at *K*' valley (even under $y \rightarrow -y$). (d) The imaginary part for the 2nd at *K*'-valley (even under $y \rightarrow -y$). The parameters we employ here are $m^* = 0.023m_e$; the MTP strength $U_0 = 165\text{meV}$ with diameter, $d = 0.663a$, where $a = 40\ \text{nm}$ is the lattice constant.

2.2 Energy bands with SOI

Now we consider the effect of spin-orbital coupling from the MTP of the system. The Hamiltonian H for the MTP lattice with SOI can be expressed by:

$$H = H_0 + H_{\mathrm{SO}} = \frac{\mathbf{p}^2}{2m^*} + V(\mathbf{r}) + H_{\mathrm{SO}}, \tag{2.7}$$

where

$$H_{\mathrm{SO}} = \frac{e\lambda}{\hbar}\boldsymbol{\sigma}\cdot(\mathbf{p}\times\mathbf{E}) = \frac{\lambda}{\hbar}\boldsymbol{\sigma}\cdot(\mathbf{p}\times\nabla V) = -\frac{\lambda}{\hbar}\boldsymbol{\sigma}\cdot(\nabla V\times\mathbf{p}), \tag{2.8 a}$$

and V is the periodic MTP expressed as $V(\mathbf{r}) = \sum_m e^{i\mathbf{G}_m\cdot\mathbf{r}}\tilde{V}_m$. Thus, we have

$$H_{\mathrm{SO}} = -\frac{\lambda}{\hbar}\boldsymbol{\sigma}\cdot(\nabla V\times\mathbf{p}) = -\frac{i\lambda}{\hbar}\sum_m e^{i\mathbf{G}_m\cdot\mathbf{r}}\tilde{V}_m\,\boldsymbol{\sigma}\cdot(\mathbf{G}_m\times\mathbf{p}). \tag{2.8 b}$$

The spin-orbit coupling constant here we employed is $\lambda = 120\text{Å}^2$, for InAs.

The wave function is in 2×1 column vector form and expressed as

$$\Psi_{\boldsymbol{\kappa}}(\mathbf{r}) = e^{i\boldsymbol{\kappa}\cdot\mathbf{r}}\sum_{m'} e^{i\mathbf{G}_{m'}\cdot\mathbf{r}}\begin{bmatrix} c_{m'\uparrow} \\ c_{m'\downarrow}\end{bmatrix}, \tag{2.9}$$

where $\uparrow$ and $\downarrow$ denote spin-up and spin-down, respectively. Thus, we have

$$\begin{aligned} H_{\mathrm{SO}}\Psi_{\boldsymbol{\kappa}}(\mathbf{r}) &= -\frac{i\lambda}{\hbar}\sum_m e^{i\mathbf{G}_m\cdot\mathbf{r}}\tilde{V}_m\boldsymbol{\sigma}\cdot(\mathbf{G}_m\times\mathbf{p})\sum_{m'} e^{i(\mathbf{G}_{m'}+\mathbf{k})\cdot\mathbf{r}}\begin{bmatrix} c_{m'\uparrow} \\ c_{m'\downarrow}\end{bmatrix} \\ &= -\frac{i\lambda}{\hbar}\sum_m e^{i\mathbf{G}_m\cdot\mathbf{r}}\tilde{V}_m\sigma_z(\mathbf{G}_m\times\mathbf{p})_z\begin{bmatrix} \sum_{m'} e^{i(\mathbf{G}_{m'}+\mathbf{k})\cdot\mathbf{r}}c_{m'\uparrow} \\ \sum_{m'} e^{i(\mathbf{G}_{m'}+\mathbf{k})\cdot\mathbf{r}}c_{n\downarrow}\end{bmatrix} \\ &= -i\lambda\sum_{m,m'} e^{i(\mathbf{G}_m+(\mathbf{G}_{m'}+\mathbf{k}))\cdot\mathbf{r}}\tilde{V}_m(\mathbf{G}_m\times(\mathbf{G}_{m'}+\mathbf{k}))_z\,\sigma_z\begin{bmatrix} c_{m'\uparrow} \\ c_{m'\downarrow}\end{bmatrix} \end{aligned} \tag{2.10}$$

In Eq.(2.10), the indexes are replaced according to the followings

$$\begin{aligned} \sum_{m\,m'} e^{i(\mathbf{G}_{m'}+\mathbf{G}_m)\cdot\mathbf{r}}\,\tilde{V}_m c_{m'} &= \sum_{m\,m''} e^{i\mathbf{G}_{m''}\cdot\mathbf{r}}\,\tilde{V}_m c_{m''-m} = \sum_{m\,m'} e^{i\mathbf{G}_{m'}\cdot\mathbf{r}}\,\tilde{V}_m c_{m'-m} \\ &= \sum_{m'\,m'''} e^{i\mathbf{G}_{m'}\cdot\mathbf{r}}\,\tilde{V}_{m'-m''}c_{m''} = \sum_{m\,m'} e^{i\mathbf{G}_m\cdot\mathbf{r}}\,\tilde{V}_{m-m'}c_{m'} \end{aligned}$$

The matrix in Eq. (2.10) is diagonal, meaning that the Hamiltonian of SOI decouples spin-up and spin-down. Therefore, we can divide the eigen-energy equation into spin-up and spin-down parts. Hence, we have the Hamiltonian equation in matrix form for a single plane-wave, $e^{i(\mathbf{k}+\mathbf{G}_{m'})\cdot\mathbf{r}}$,

$$\left\{\frac{\hbar^2\left|\mathbf{k}+\mathbf{G}_{m'}\right|^2}{2m^*}+\sum_m \tilde{V}_{m'-m}\left(\mathbf{1}-i\lambda\left[\mathbf{G}_{m'-m}\times\left(\mathbf{G}_m+\mathbf{k}\right)\right]\sigma_z\right)\right\}\begin{bmatrix}c_{m\uparrow}\\ c_{m\downarrow}\end{bmatrix}=E\begin{bmatrix}c_{m'\uparrow}\\ c_{m'\downarrow}\end{bmatrix} \qquad (2.11)$$

By Eq. (2.11), we compare the band structures with/without SOI and display the results in Fig. 2.4. The SOI turns the system into an insulator (introduces an energy gap at the Dirac point). Furthermore, the system behaviors as a Z_2 topological insulator [12]. In the following chapters, we will discuss the effects on the topological properties from external magnetic field.

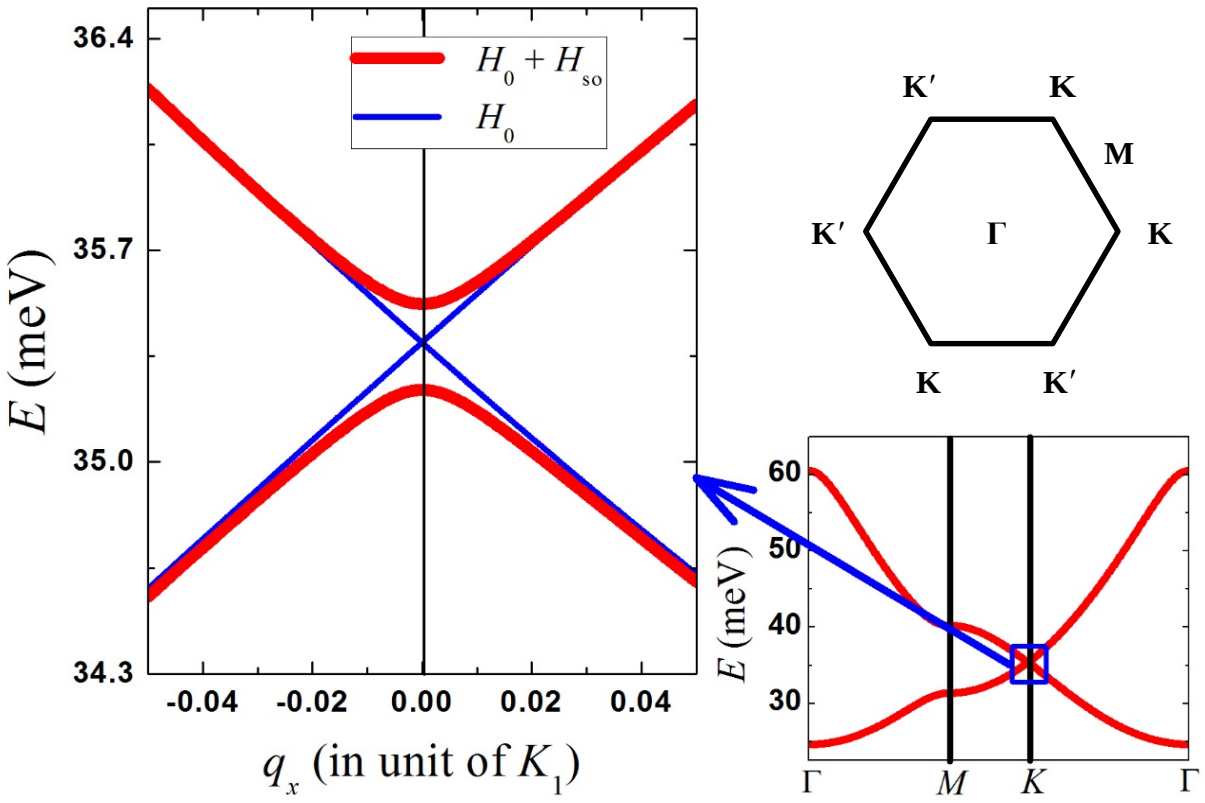

Fig. 2.4: The lowest two bands for the 2DEG subjected to MTP lattice. The blues lines are those without SOI, while the red lines are those with SOI. Apparently, the SOI introduces the energy gap at *K* and *K*' points. For symmetric reason, the band structures near *K*' point is not shown here. The parameters we employ here are $m^* = 0.023m_e$; the MTP strength $U_0 = 165\text{meV}$ with diameter, $d = 0.663a$, where $a = 40\,\text{nm}$ is the lattice constant. The SOI coupling constant is $\lambda = 120\text{Å}^2$.

2.3 The $\mathbf{k}\cdot\mathbf{p}$ theory at *K*- and *K'*- valley

Since we are only interested in the band structures near *K* and *K'* points, we want to develop the effective theory that fits the lowest two bands near these two symmetry points. Here we adopt the following notations: the wave vector, $\mathbf{k}=\tau\mathbf{K}+\mathbf{q}$, near τK point , with $|\mathbf{q}|\ll|\mathbf{K}|$. The valley index $\tau=+1$ and -1, denotes *K*- and *K'*- valleys, respectively. From the Schrödinger equation

$$\left[-\frac{\hbar^2}{2m^*}\nabla^2+V(\mathbf{r})+H_{\mathrm{SO}}\right]\varphi_{\mathbf{k}}(\mathbf{r})=\varepsilon\varphi_{\mathbf{k}}(\mathbf{r}), \tag{2.12}$$

with wave-function in Bloch form, $\varphi_{\mathbf{k}}(\mathbf{r})=e^{i\mathbf{k}\cdot\mathbf{r}}u_{\mathbf{k}}(\mathbf{r})=e^{i(\tau\mathbf{K}+\mathbf{q})\cdot\mathbf{r}}u_{\mathbf{k}}(\mathbf{r})$. The kinetic term in the LHS of Eq. (2.12) is replaced by

$$\begin{aligned}
-\frac{\hbar^2}{2m^*}\nabla^2 e^{i(\tau\mathbf{K}+\mathbf{q})\cdot\mathbf{r}}u_{\mathbf{k}}(\mathbf{r}) &= -\frac{\hbar^2}{2m^*}e^{i(\tau\mathbf{K}+\mathbf{q})\cdot\mathbf{r}}\left|i\left(\tau\mathbf{K}+\mathbf{q}\right)+\nabla\right|^2 u_{\mathbf{k}}(\mathbf{r})\\
&= -e^{i(\tau\mathbf{K}+\mathbf{q})\cdot\mathbf{r}}\frac{\hbar^2}{2m^*}\left\{\left|i\tau\mathbf{K}+\nabla\right|^2+2\left(i\tau\mathbf{K}+\nabla\right)\cdot i\mathbf{q}-q^2\right\}u_{\mathbf{k}}(\mathbf{r})\\
&= e^{i(\tau\mathbf{K}+\mathbf{q})\cdot\mathbf{r}}\left\{-\frac{\hbar^2\left|i\tau\mathbf{K}+\nabla\right|^2}{2m^*}-\frac{\hbar^2}{m^*}\left(i\tau\mathbf{K}+\nabla\right)\cdot i\mathbf{q}+\frac{\hbar^2 q^2}{2m^*}\right\}u_{\mathbf{k}}(\mathbf{r})\\
&\simeq e^{i(\tau\mathbf{K}+\mathbf{q})\cdot\mathbf{r}}\left\{\frac{\left|\hbar\tau\mathbf{K}+\hat{\mathbf{p}}\right|^2}{2m^*}+\frac{\hbar}{m^*}\left(\hbar\tau\mathbf{K}+\hat{\mathbf{p}}\right)\cdot\mathbf{q}\right\}u_{\mathbf{k}}(\mathbf{r})
\end{aligned} \tag{2.13}$$

Since q is small compared with $\mathbf{K}$, the quadratic term in Eq. (2.13) is neglected. Thus Eq. (2.12) is approximated accordingly,

$$\begin{aligned}
&\left[-\frac{\hbar^2}{2m^*}\nabla^2+V(\mathbf{r})+H_{\mathrm{SO}}\right]\varphi_{\mathbf{k}}(\mathbf{r})\\
&\simeq e^{i(\tau\mathbf{K}+\mathbf{q})\cdot\mathbf{r}}\left\{\begin{array}{l}\dfrac{\left|\hbar\tau\mathbf{K}+\hat{\mathbf{p}}\right|^2}{2m^*}+V(\mathbf{r})+\\ \dfrac{\hbar}{m^*}\left(\hbar\tau\mathbf{K}+\hat{\mathbf{p}}\right)\cdot\mathbf{q}+H_{\mathrm{SO}}(\tau\mathbf{K}+\mathbf{q})\end{array}\right\}u_{\mathbf{k}}(\mathbf{r})\\
&\simeq e^{i(\tau\mathbf{K}+\mathbf{q})\cdot\mathbf{r}}\left[H_0\left(\tau\mathbf{K}\right)+H_{\mathbf{q}}(\tau\mathbf{K})\cdot\mathbf{q}+H_{\mathrm{SO}}(\tau\mathbf{K})\right]u_{\mathbf{k}}(\mathbf{r})\\
&=\varepsilon e^{i(\tau\mathbf{K}+\mathbf{q})\cdot\mathbf{r}}u_{\mathbf{k}}(\mathbf{r}).
\end{aligned} \tag{2.14a}$$

Here $H_0(\tau\mathbf{K})=\frac{|\hbar\tau\mathbf{K}+\hat{\mathbf{p}}|^2}{2m^*}+V(\mathbf{r})$ is treated as the unperturbed Hamiltonian, while

$$H_{\mathbf{q}}(\tau\mathbf{K})\cdot\mathbf{q}=\frac{\hbar}{m^*}\left(\hbar\tau\mathbf{K}+\hat{\mathbf{p}}\right)\cdot\mathbf{q}$$

and $H_{\mathrm{SO}}(\tau\mathbf{K})$ are the perturbation. In Eq. (2.14), the SOI Hamiltonian is approximated

as $H_{\mathrm{SO}}(\tau\mathbf{K}+\mathbf{q}) \cong H_{\mathrm{SO}}(\tau\mathbf{K})$ since the remainder is of the order of q^2. Drop the common phase term in both sides, and express Eq. (2.14a) in the operator form

$$\left[H_0(\tau\mathbf{K}) + H_{\mathbf{q}}(\tau\mathbf{K})\cdot\mathbf{q} + H_{\mathrm{SO}}(\tau\mathbf{K})\right]\left|n,\tau\mathbf{K}+\mathbf{q};\mu\right\rangle = \varepsilon_n(\mathbf{q})\left|n,\tau\mathbf{K}+\mathbf{q};\mu\right\rangle \quad (2.14b)$$

where μ labels the spin degrees of freedom that $|n,\tau\mathbf{K}+\mathbf{q};\mu\rangle = |n,\tau\mathbf{K}+\mathbf{q}\rangle\otimes|\mu\rangle$. The eigen-states of $H_0(\tau\mathbf{K})$ form the complete set, $\{|n,\tau;\mu\rangle_0 = |n,\tau\rangle\otimes|\mu\rangle\}$, saying

$$\left|n,\tau\mathbf{K}+q;\mu\right\rangle = \sum_{n',\mu'} c^{(n)}_{n',\mu'}(\mathbf{q})\left|n,'\tau;\mu'\right\rangle \quad (2.15)$$

with $\{|n,\tau;\mu\rangle\}$ satisfying the eigen-value equation,

$$H_0(\tau\mathbf{K})\left|n,\tau;\mu\right\rangle = \varepsilon_{n,\mu}(\tau\mathbf{K})\left|n,\tau;\mu\right\rangle.$$

Here n denotes the band index and $\mu = \pm 1$ denote spin-up and spin-down states.

By restricting only lowest four degenerate states (including spin) in Eq. (2.15), saying $\{|n,\tau;\mu\rangle\} = \{|1,\tau;+\rangle, |2,\tau;+\rangle, |1,\tau;-\rangle, |2,\tau;-\rangle\}$ being the basis set we considering, the matrix form of Eq. (2.14b) would be

$$\begin{pmatrix} \varepsilon_0+\tau h_x q_x & \tau h_y q_y - i\lambda_{\mathrm{SO}} & 0 & 0 \\ \tau h_y q_y + i\lambda_{\mathrm{SO}} & \varepsilon_0 - \tau h_x q_x & 0 & 0 \\ 0 & 0 & \varepsilon_0+\tau h_x q_x & \tau h_y q_y + i\lambda_{\mathrm{SO}} \\ 0 & 0 & \tau h_y q_y - i\lambda_{\mathrm{SO}} & \varepsilon_0 - \tau h_x q_x \end{pmatrix} \begin{pmatrix} c^{(n)}_{1,+} \\ c^{(n)}_{2,+} \\ c^{(n)}_{1,-} \\ c^{(n)}_{2,-} \end{pmatrix} = \varepsilon_n \begin{pmatrix} c^{(n)}_{1,+} \\ c^{(n)}_{2,+} \\ c^{(n)}_{1,-} \\ c^{(n)}_{2,-} \end{pmatrix}. \quad (2.17)$$

The matrix in Eq. (2.17) is Block-diagonal since spin-up and spin-down are decoupled even in the presence of SOI. Besides, the energy ε_0 in the diagonal element is independent of valley and spin that $\langle n',\tau;\mu'|\hat{H}_0(\tau\mathbf{K})|n,\tau;\mu\rangle = \varepsilon_0\delta_{n,n'}\delta_{\mu,\mu'}$. The numerically determined constants h_x, h_y, and λ_{SO} are all real, positive, and **q**- and, also, τ-independent. First of all, h_x and h_y, are defined through

$$\begin{aligned} \left\langle n,\tau;\mu\left|\hat{H}_{\mathbf{q}}(\tau\mathbf{K})\cdot\hat{x}q_x\right|n',\tau;\mu'\right\rangle &= \tfrac{\hbar}{m^*}\left\langle n,\tau\left|\left(\hbar\tau\mathbf{K}+\hat{\mathbf{p}}\right)\cdot\hat{x}\right|n',\tau\right\rangle q_x\delta_{\mu,\mu'} \\ &= \tfrac{\hbar}{m^*}\left\langle n,\tau\left|\left(\hbar\tau K+\hat{p}_x\right)\right|n',\tau\right\rangle q_x\delta_{\mu,\mu'} \\ &= q_x\left(h_0\hat{\pi}_0 + h_3\hat{\pi}_z\right)\delta_{\mu,\mu'} \end{aligned} \quad (2.18a)$$

$$\begin{aligned} \left\langle n,\tau;\mu\left|\hat{H}_{\mathbf{q}}(\tau\mathbf{K})\cdot\hat{y}q_y\right|n',\tau;\mu'\right\rangle &= \tfrac{\hbar}{m^*}\left\langle n,\tau\left|\left(\hbar\tau\mathbf{K}+\hat{\mathbf{p}}\right)\cdot\hat{y}\right|n',\tau\right\rangle q_y\delta_{\mu,\mu'} \\ &= \tfrac{\hbar}{m^*}\left\langle n,\tau\left|\hat{p}_y\right|n',\tau\right\rangle q_y\delta_{\mu,\mu'} \\ &= q_y\left(h_1\hat{\pi}_x + h_2\hat{\pi}_y\right)\delta_{\mu,\mu'} = q_y h_1\hat{\pi}_x\delta_{\mu,\mu'}, \end{aligned} \quad (2.18b)$$

where π_0 and $\{\pi_x,\pi_y,\pi_z\}$ are the 2×2 identity and Pauli matrices for the space spanned by $\{|1,\tau\rangle, |2,\tau\rangle\}$, alone with σ_0 and $\{\sigma_x,\sigma_y,\sigma_z\}$ being those matrices for the spin degrees of freedom. In Eq. (2.18), the symmetry properties that $|1,\tau,\pm\rangle \to -|1,\tau,\pm\rangle$ and $|2,\tau;\pm\rangle \to |2,\tau;\pm\rangle$ under $y\to -y$ are employed. Similarly,

$$\hat{H}_{\mathbf{q}}(\tau\mathbf{K}) = \frac{\hbar}{m^*}(\tau\hbar K + \hat{p}_x, \hat{p}_y) \longrightarrow \frac{\hbar}{m^*}(\tau\hbar K + \hat{p}_x, -\hat{p}_y)$$

under the same symmetry transform. Such symmetry relations restrict the matrix elements, in Eq. (2.18a), depending on π_0 and π_3, while only π_1 and π_2 are presence in Eq. (2.18b), leaving the expansion coefficients h_0, h_1, h_2, and h_3, which are all real due to the Hermitian of $\hat{H}_{\mathbf{q}}(\tau\mathbf{K}) \cdot \mathbf{q}$. On the other hand, the matrix elements, $\langle n, \tau; \mu | \hat{H}_{\mathbf{q}}(\tau\mathbf{K}) \cdot \mathbf{q} | n', \tau; \mu' \rangle$, are also real (for details, see **Appendix B**), it immediately infers that $h_2 = 0$. Therefore we reach the result that

$$\langle n, \tau; \mu | \hat{H}_0(\tau\mathbf{K}) + \hat{H}_{\mathbf{q}}(\tau\mathbf{K}) \cdot \mathbf{q} | n', \tau; \mu' \rangle = \{(\varepsilon_0 + q_x h_0)\hat{\pi}_0 + q_x h_3 \hat{\pi}_z + q_y h_1 \hat{\pi}_x\} \delta_{\mu,\mu'}.$$

The eigen-energies of the above Hamiltonian are

$$\varepsilon(\mathbf{q}) = \varepsilon_0 + h_0 q_x \pm \sqrt{h_3^2 q_x^2 + h_1^2 q_y^2}$$

However, the C_3-rotation symmetry at $\tau\mathbf{K}$ requires $h_0 = 0$ and $|h_3| = |h_1|$ to have the energy replicating the 3-fold rotation symmetry of the bands. These help us to further simplify Eq. (2.18):

$$\begin{aligned} \langle n, \tau; \mu | \hat{H}_{\mathbf{q}}(\tau\mathbf{K}) \cdot \hat{x} q_x | n', \tau; \mu' \rangle &= q_x h_3 \hat{\pi}_z \delta_{\mu,\mu'} = \tau h_x q_x \hat{\pi}_z \otimes \hat{\sigma}_0; \\ \langle n, \tau; \mu | \hat{H}_{\mathbf{q}}(\tau\mathbf{K}) \cdot \hat{y} q_y | n', \tau; \mu' \rangle &= q_y h_1 \hat{\pi}_x \delta_{\mu,\mu'} = \tau h_y q_y \hat{\pi}_x \otimes \hat{\sigma}_0 \end{aligned} \tag{2.19}$$

by defining $\tau h_x \equiv h_3$ and $\tau h_y \equiv h_1$ with h_x and h_y are τ-*independent* constants, and $|h_x| = |h_y|$. The valley dependence (τ-dependence) of these matrix elements is discussed in **Appendix B**, and here we just employ the results.

The other numerical determined constant, λ_{SO}, is defined through the SOI Hamiltonian, $\hat{H}_{\mathrm{SO}} = \hat{V}_{\mathrm{SO}} \otimes \hat{\sigma}_z$, saying

$$\langle n, \tau; \mu | \hat{H}_{\mathrm{SO}} | n', \tau; \mu' \rangle = \langle n, \tau | \hat{V}_{\mathrm{SO}} | n', \tau \rangle \delta_{\mu,\mu'} = \lambda_{\mathrm{SO}} \hat{\pi}_y \otimes \hat{\sigma}_z. \tag{2.20}$$

The matrix elements, $\langle n, \tau | \hat{V}_{\mathrm{SO}} | n', \tau \rangle$ which is τ-*independent*, and again, is represented by $\hat{\pi}_y$ (details are shown in **Appendix B**).

In summary, we have

$$\begin{aligned} h_x &= \tfrac{\hbar}{m^*} \langle 1, \tau = 1 | (\hbar\mathbf{K} + \hat{\mathbf{p}}) \cdot \hat{x} | 1, \tau = 1 \rangle = -\tfrac{\hbar}{m^*} \langle 2, \tau = 1 | (\hbar\mathbf{K} + \hat{\mathbf{p}}) \cdot \hat{x} | 2, \tau = 1 \rangle; \\ h_y &= \tfrac{\hbar}{m^*} \langle 1, \tau = 1 | \hat{\mathbf{p}} \cdot \hat{y} | 2, \tau = 1 \rangle = \tfrac{\hbar}{m^*} \langle 2, \tau = 1 | \hat{\mathbf{p}} \cdot \hat{y} | 1, \tau = 1 \rangle; \\ \lambda_{\mathrm{SO}} &= i \langle 1, \tau = 1 | \hat{V}_{\mathrm{SO}} | 2, \tau = 1 \rangle. \end{aligned}$$

which are all valley (τ) independent. From numerical calculation, we found $h_x = h_y = h = 0.5088\,\hbar^2 K_0/(2m^*)$, while $\lambda_{\mathrm{SO}} = 0.0026\,\hbar^2 K_0^2/(2m^*)$. Therefore we arrive the $\mathbf{k} \cdot \mathbf{p}$ effective Hamiltonian with positive-definite and valley-independent parameters,

ε_0, λ_{SO}, and h.

$$\begin{pmatrix} \varepsilon_0+\tau h q_x & \tau h q_y - i\lambda_{\mathrm{SO}} & 0 & 0 \\ \tau h q_y + i\lambda_{\mathrm{SO}} & \varepsilon_0 - \tau h q_x & 0 & 0 \\ 0 & 0 & \varepsilon_0+\tau h q_x & \tau h q_y + i\lambda_{\mathrm{SO}} \\ 0 & 0 & \tau h q_y - i\lambda_{\mathrm{SO}} & \varepsilon_0 - \tau h q_x \end{pmatrix} \begin{pmatrix} c_{1.+}^{(n)} \\ c_{2.+}^{(n)} \\ c_{1.-}^{(n)} \\ c_{2.-}^{(n)} \end{pmatrix} = \varepsilon_n \begin{pmatrix} c_{1.+}^{(n)} \\ c_{2.+}^{(n)} \\ c_{1.-}^{(n)} \\ c_{2.-}^{(n)} \end{pmatrix}, \quad (2.21)$$

and the eigen-energies are

$$\varepsilon_\eta(q) = \eta\sqrt{\lambda_{so}^2 + h^2 q^2} \quad (2.22)$$

which are 2-fold degeneracy with $\eta = \pm 1$, characterizing the upper and lower branches. At $q = 0$, i.e. exact on $\tau\mathbf{K}$-point, $\varepsilon_\eta = \eta|\lambda_{\mathrm{SO}}|$. Therefore the SOI open up an energy gap on $\tau\mathbf{K}$-point, with the gap of $2|\lambda_{\mathrm{SO}}|$. The energy band structures of the $\mathbf{k}\cdot\mathbf{p}$ theory is shown in Fig. 2.5, which is consistent with those bands shown in **Sec. 2.2**.

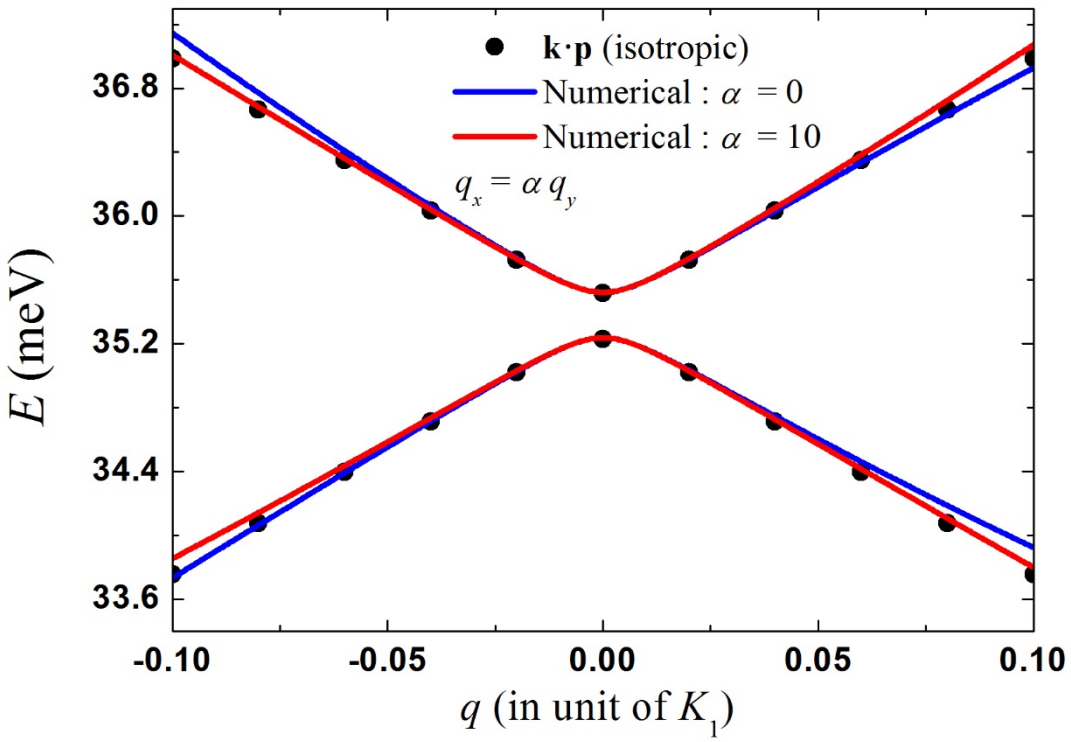

Fig. 2.5 The band structures along different **q**-directions (different α values). Comparing with the numerical results (the solid blue and red lines), the $\mathbf{k}\cdot\mathbf{p}$ theory (isotropic band structures, independent of α) is accurate. The parameters we employ here are $m^* = 0.023m_e$; the MTP strength $U_0 = 165$meV with diameter $d = 0.663a$, and $a = 40$ nm is the lattice constant. The SOI coupling constant is $\lambda = 120\text{Å}^2$

From the result in Fig. 2.5, the effective theory derived in this section has good approximation to the band structure around *K*- and *K'*- valley. Therefore, in the following chapters, we can develop the band structure in the presence of magnetic field (**Chapter 3**) and the topologies properties for our system (**Chapter 4**) by means of this effective theory.

Chapter 3

Energy bands with SOI and magnetic field

In this chapter, we start discussion by the band structures of 2DEG in MTP lattice with SOI and in-plane magnetic field (**Sec.** 3.1). From previous chapter, the SOI introduces the energy gap at the *K*- and *K'*- valley for the lower bands, seeing the spin-up and spin-down state along z-direction. The effect of in-plane magnetic field produces laterally sift and leaves the degenerate points at *K*- and *K'*-valley. Then we consider in-plane and out-of-magnetic field simultaneously (**Sec.** 3.2). The strength of the out-of-plane magnetic field is small enough so that it wouldn't have influence on the motion of electrons. The effect of out-of-plane magnetic field produces longitudinal energy shift at the degenerate points in **Sec.** 3.1. In **Sec.** 3.3 we develop the perturbation method and low energy effective theory around *K*- and *K'*-valley separately.

3.1 Energy bands with SOI and in-plane magnetic field

The Hamiltonian for the muffin-tin lattice with SOI and in-plane magnetic field can be expressed by:

$$H = H_0 + H_{\mathrm{SO}} + H_{\mathrm{B}} = \frac{\mathbf{p}^2}{2m^*} + V(\mathbf{r}) + H_{\mathrm{SO}} + H_{\parallel}, \tag{3.1}$$

where $\hat{H}_{\mathrm{SO}}$ is the SOI Hamiltonian shown in Eq. (2.8), and $\hat{H}_{\parallel}$ is the Zeeman term introduced by in-plane magnetic field.

$$\hat{H}_{\parallel} = g\mu_{\mathrm{B}}\mathbf{s}\cdot\mathbf{B}_{\parallel}.$$

Here g is the g-factor and is equal to 2; $\mu_{\mathrm{B}} = 9.27\times10^{-24}(J\cdot T^{-1})$ is the Bohr magneton; $\mathbf{s} = \frac{\hbar}{2}\boldsymbol{\sigma}$ with $\boldsymbol{\sigma}$ being the vector Pauli matrices, and $\mathbf{B}_{\parallel} = \mathrm{B}_x\hat{x}+\mathrm{B}_y\hat{y}$ is the in-plane magnetic field.

As the derivation of the matrix equation without in-plane magnetic field discussed in **Chapter** 2, we can obtain the equation with in-plane magnetic field in matrix form:

$$\sum_{m'} e^{i\mathbf{k}\cdot\mathbf{r}} e^{i\mathbf{G}_{m'}\cdot\mathbf{r}} \left[\frac{\hbar^2}{2m^*}\left|\mathbf{k}+\mathbf{G}_{m'}\right|^2\right]\begin{bmatrix} c_{m'\uparrow} \\ c_{m'\downarrow}\end{bmatrix}$$
$$+\sum_{m'm} e^{i\mathbf{k}\cdot\mathbf{r}} e^{i\mathbf{G}_{m'}\cdot\mathbf{r}} \tilde{V}_{m'-m}\left\{1-i\lambda\sigma_z\left[\mathbf{G}_{m'-m}\times\left(\mathbf{G}_{m'}+\mathbf{k}\right)\right]_z\right\}\begin{bmatrix} c_{m'\uparrow} \\ c_{m'\downarrow}\end{bmatrix} \quad (3.2a)$$
$$+\sum_{m'} e^{i\mathbf{k}\cdot\mathbf{r}} e^{i\mathbf{G}_{m'}\cdot\mathbf{r}} \frac{1}{2} g\mu_{\mathrm{B}}\left(B_x\sigma_x+B_y\sigma_y\right)\begin{bmatrix} c_{m'\uparrow} \\ c_{m'\downarrow}\end{bmatrix} = E\sum_{m'} e^{i\mathbf{k}\cdot\mathbf{r}} e^{i\mathbf{G}_{m'}\cdot\mathbf{r}}\begin{bmatrix} c_{m'\uparrow} \\ c_{m'\downarrow}\end{bmatrix}$$

In the second term in Eq. (3.2a), the index relabeling has been performed implicitly. We define $\mathbf{G}_{m''}=\mathbf{G}_{m'}+\mathbf{G}_m$, and $m=m''-m'$, and replace m'' by m' in the final step. Specifically,

$$\sum_{mm'} e^{i\mathbf{k}\cdot\mathbf{r}} e^{i(\mathbf{G}_{m'}+\mathbf{G}_m)\cdot\mathbf{r}}\,\tilde{V}_m c_{m'} = \sum_{m'm''} e^{i\mathbf{k}\cdot\mathbf{r}} e^{i\mathbf{G}_{m''}\cdot\mathbf{r}}\,\tilde{V}_{m''-m'} c_{m'} = \sum_{mm'} e^{i\mathbf{k}\cdot\mathbf{r}} e^{i\mathbf{G}_{m'}\cdot\mathbf{r}}\,\tilde{V}_{m'-m} c_{m'} \quad (3.2\text{ b})$$

Finally, we arrive the equation for a general plane-wave $e^{i(\mathbf{k}+\mathbf{G}_n)\cdot\mathbf{r}}$,

$$\sum_m \begin{bmatrix} \frac{\hbar^2}{2m^*}\left|\mathbf{k}+\mathbf{G}_m\right|^2\delta_{mm'}+\tilde{V}_{m'-m}\left\{1-i\lambda\sigma_z\left[\mathbf{G}_{m'-m}\times\left(\mathbf{G}_m+\mathbf{k}\right)\right]_z\right\} \\ +\frac{1}{2}g\mu_{\mathrm{B}}\left(B_x\sigma_x+B_y\sigma_y\right)\delta_{mm'}\end{bmatrix}\begin{bmatrix} c_{m\uparrow} \\ c_{m\downarrow}\end{bmatrix} = E\begin{bmatrix} c_{m'\uparrow} \\ c_{m'\downarrow}\end{bmatrix} \quad (3.3)$$

For the absence of $\mathbf{B}_{\parallel}$, the spin-up and -down are good quantum number, however, the in-plane magnetic field mixes them up. In other words, the orientations of spin-up and spin-down state in Eq. (3.3) are not in the z-direction anymore. We cannot divide Eq. (3.3) into spin-up & down equation after applying the in-plane magnetic field. Furthermore, we use two group of indices to label the Hamiltonian matrices, $M_{mm'}^{\eta\eta'}$, in Eq. (3.3): where $\eta,\eta'=\uparrow$ and $\downarrow$ stand for the spin indices while *n* and *m* label the plane-wave index. The explicit form of $M_{mm'}^{\eta\eta'}$ can be expressed by:

$$M_{mm'}^{\eta\eta'}=\frac{\hbar^2}{2m^*}\left|\mathbf{k}+\mathbf{G}_m\right|^2\delta_{mm'}\delta_{\eta\eta'}+\tilde{V}_{m'-m}\left\{1-i\lambda\left[\mathbf{G}_{m'-m}\times\left(\mathbf{G}_m+\mathbf{k}\right)\right]\right\}\delta_{\eta\eta'}$$
$$+\left[\frac{1}{2}g\mu_{\mathrm{B}}\left(B_x+i\bar{\eta}B_y\right)\right]\delta_{mm'}\delta_{\eta\bar{\eta}'}$$

Eq. (3.3) is in the compact matrix form

$$\begin{bmatrix} & M_{mm'}^{\eta\eta'} & \end{bmatrix}\begin{bmatrix} c_{m\eta'}\end{bmatrix} = E\begin{bmatrix} c_{m'\eta}\end{bmatrix}$$

Since we only address the low energy band features, Fig. 3.1 shows the low energy band structures around *K* point with $\mathbf{B}_{\parallel}$ and also without $\mathbf{B}_{\parallel}$ for comparison. For band structures with a wider energy range are shown in **Appendix C**. From Fig. 3.1, we find that the spin-up and spin-down degeneracy in the absence of $\mathbf{B}_{\parallel}$ is removed by magnetic field, resulting in four separated bands. Furthermore, there are doubly two-

fold degeneracy exact at *K* point. Such degeneracy plays some crucial role in the band topology which will be discussed in next chapter. In **Appendix D**, we will demonstrate the degeneracy by symmetry argument.

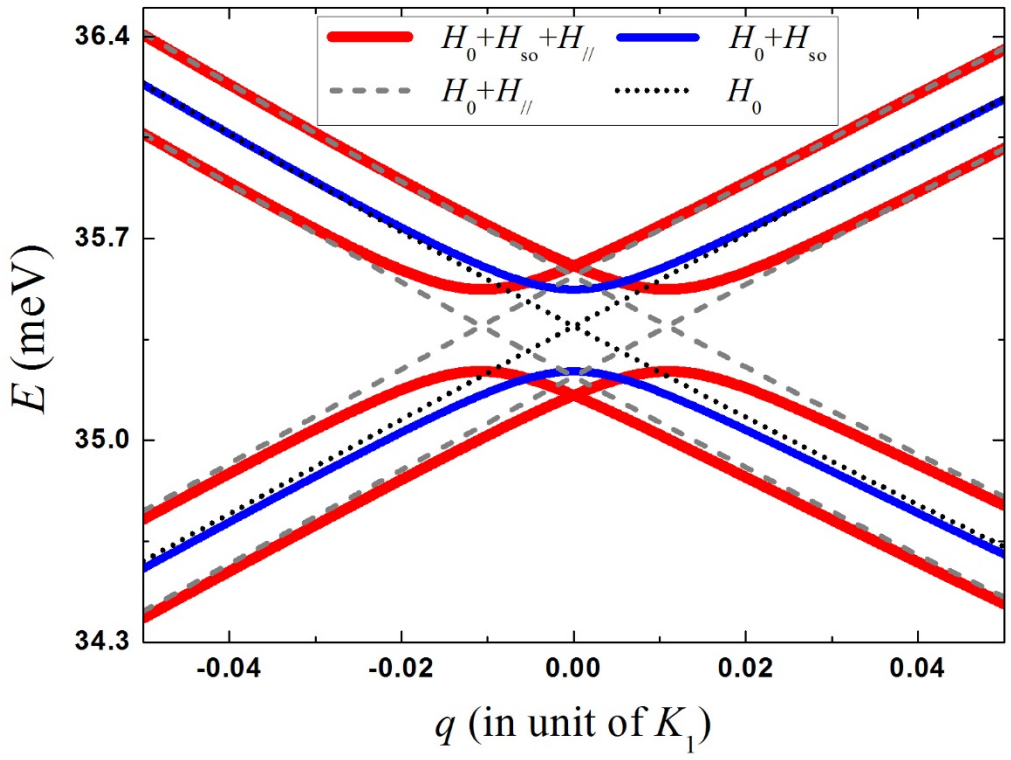

Fig. 3.1 The lowest four bands of 2DEG subjected to MTP lattice. The blue solid lines (double degenerate) are those with $\mathbf{B}_{\parallel} = 0$T, while the red solid lines are those with $\mathbf{B}_{\parallel} = 3$T. The SOI is present for both of them. For comparison, the band structures without SOI but with $\mathbf{B}_{\parallel} = 0$T (black dotted lines) and $\mathbf{B}_{\parallel} = 3$T (gray dashed lines) are also shown. The other parameters we employ here are λ =120 Å^2 (InAs); $m^* = 0.023m_e$; $U_0 = 165$meV; $a = 40$nm; $d = 0.663a$.

From the numerical results in Fig. 3.2a and 3.2b, under in-plane magnetic field, the lowest two bands split laterally into four bands and have two degenerate points at *K* point. The scale of the energy gap between the degenerate points is proportional to the strength of the applied field. However, for the doubly two-fold degeneracy bands, the degeneracy at *K* point has robustness against the strength of in-plane magnetic field. In other words, no matter what the in-plane magnetic field strength is, the crossing type of the two degenerate points must be crossing in stead of anti-crossing (for detail, see **Appendix D**).

3.2 Energy bands with SOI and general magnetic field

In this section, we generalize the direction of magnetic field. That is, besides an in-plane field, $\mathbf{B}_{\parallel}$, a small out-of plane magnetic field, $\mathbf{B}_{\perp}$, is also applied simultaneously. Since $|\mathbf{B}_{\perp}| \ll |\mathbf{B}_{\parallel}|$, we assume the electrons motion would not be affected by out-of-plane field. Hence we could neglect the vector potential and consider only Zeeman effect. The Hamiltonian of Zeeman term becomes:

$$\hat{H}_{\mathrm{B}} = g\mu_{\mathrm{B}}\mathbf{s}\cdot\mathbf{B} = \frac{1}{2}g\mu_{\mathrm{B}}\boldsymbol{\sigma}\cdot\left(\mathbf{B}_{\parallel}+\mathbf{B}_{\perp}\right) = \frac{1}{2}g\mu_{\mathrm{B}}\left(B_z\sigma_z + B_x\sigma_x + B_y\sigma_y\right), \tag{3.5}$$

with $\mathbf{B}_{\parallel} = \mathrm{B}_x\hat{x}+\mathrm{B}_y\hat{y}$, $\mathbf{B}_{\perp} = \mathrm{B}_z\hat{z}$

Substitute Eq. (3.5) into the Eq. (3.1), after calculation in **Sec.** 3.1 the total Hamiltonian matrices under general magnetic field is:

$$\sum_m \begin{bmatrix} \frac{\hbar^2}{2m^*}\left|\mathbf{k}+\mathbf{G}_m\right|^2\delta_{mm'} + \tilde{V}_{m'-m}\left\{1-i\lambda\sigma\left[\mathbf{G}_{m'-m}\times\left(\mathbf{G}_m+\mathbf{k}\right)\right]_z\right\} \\ +\frac{1}{2}g\mu_{\mathrm{B}}\left(B_z\sigma_z+B_x\sigma_x+B_y\sigma_y\right)\delta_{m'm} \end{bmatrix} \begin{bmatrix} c_{m\uparrow} \\ c_{m\downarrow} \end{bmatrix} = E\begin{bmatrix} c_{m'\uparrow} \\ c_{m'\downarrow} \end{bmatrix} \tag{3.6}$$

The matrix equation in Eq. (3.6) can be written in the following form:

$$\begin{bmatrix} \\ M_{mm'}^{\eta\eta'} \\ \\ \end{bmatrix}\begin{bmatrix} \\ c_{m\eta'} \\ \\ \end{bmatrix} = E\begin{bmatrix} \\ c_{m'\eta} \\ \\ \end{bmatrix}$$

where $\eta,\eta' = \uparrow\downarrow$(↑: spin-up, ↓: spin-down), the explicit form of $M_{mm'}^{\eta\eta'}$ is:

$$M_{mm'}^{\eta\eta'} = \left[\frac{\hbar^2}{2m^*}\left|\mathbf{k}+\mathbf{G}_m\right|^2 + \frac{1}{2}g\mu_{\mathrm{B}}B_z\right]\delta_{mm'}\delta_{\eta\eta'} + \tilde{V}_{m'-m}\left\{1-i\lambda\left[\mathbf{G}_{m'-m}\times\left(\mathbf{G}_m+\mathbf{k}\right)\right]\right\}\delta_{\eta\eta'}$$
$$+\left[\frac{1}{2}g\mu_{\mathrm{B}}\left(B_x+i\bar{\eta}B_y\right)\right]\delta_{mm'}\delta_{\eta\bar{\eta}'}$$

The energy band structure under the general magnetic field at *K* point is shown in **Fig.** 3.2. Distinguish from the effect of in-plane magnetic field, out-of-plane magnetic field gives longitudinally energy shifts at *K* point. The band structure under the in-plane magnetic field (**Sec.** 3.1) degenerates at *K* point. With the effect of the small out-of-plane magnetic field, this band structure would open gaps at the originally degenerate points.

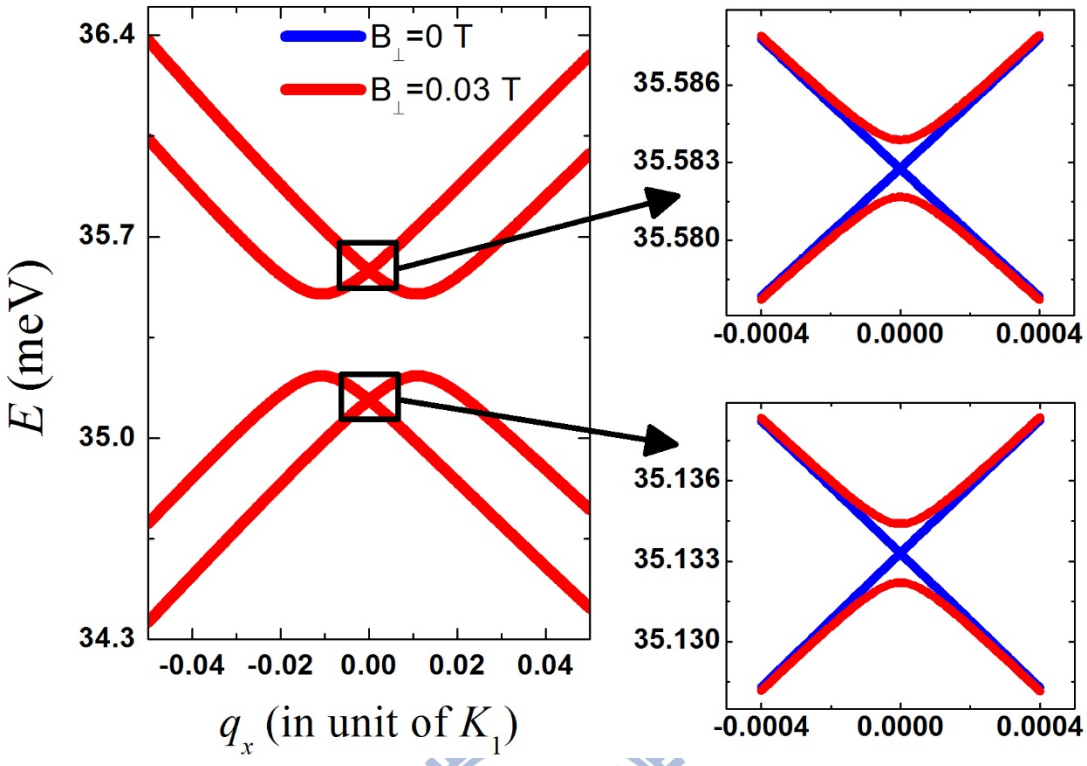

Fig. 3.2: The lowest four bands around *K* point of 2DEG subjected to MTP lattice. The blue lines are those with $\mathbf{B}_\perp = 0$T while the red lines are those with $\mathbf{B}_\perp = 0.03$T. The in-plane magnetic field is $\mathbf{B}_\parallel = 3$T for both of them. The other parameters we use here are λ =120 Å^2 (InAs); $m^* = 0.023m_e$; $U_0 = 165$meV; $a = 40$nm; $d = 0.663a$.

From **Chapter** 2, without SOI and magnetic field the lowest two bands degenerate at *K* point (**Fig.** 2.1). After considering the effect of SOI, the degeneracy at *K* point is broken, opening an energy gap. Furthermore we add external magnetic field to our system in this chapter. The effect of magnetic field produces energy splits, lateral (in-plane magnetic field) and longitudinal (out-of-plane magnetic field) energy shifts. Furthermore, according to **Sec. 3.1**, the in-plane magnetic field leads to lateral energy split and gives two degenerate points at *K*-valley for the lowest two bands. These degenerate states at *K*-valley remain robustness against the strength of the in-plane magnetic field, and they cannot open a gap even coupling higher bands via SOI. However, in this section, the small out-of-plane magnetic field produces longitudinal energy shifts and breaks the degeneracy mentioned in **Sec. 3.1**. From the previous results, we find that the band structure and degeneracy at *K*- (and *K'-)* valley could be adjusted through turning on/off SOI or magnetic field; additionally, there are the appearance of topological variation simultaneously. About the topological properties of our system would be discussed in the next chapter.

3.3 Effect theory at *K*- and *K'*- valley

In this section, we base on the $\mathbf{k}\cdot\mathbf{p}$ theory discussed in Sec. 2.4, and develop the effective theory of *K*- and *K'*- valley, which will be utilized in the analysis the topology of these bands in next chapter. First of all, the Zeeman term, $\hat{H}_B = \hat{H}_{\parallel} + \hat{H}_{\perp}$, is separated into $\hat{H}_{\parallel}$ and $\hat{H}_{\perp}$, with

$$\hat{H}_{\parallel} = \tfrac{1}{2} g\mu_B \hat{\boldsymbol{\sigma}}\cdot\mathbf{B}_{\parallel}, \text{ and}$$
$$\hat{H}_{\perp} = \tfrac{1}{2} g\mu_B \hat{\sigma}_z B_{\perp}, \text{ with}$$
$$\mathbf{B} = \mathbf{B}_{\parallel} + B_{\perp}\hat{z}$$

The Hamiltonian of the system is $\hat{H}(\mathbf{k}) = \hat{H}_0(\mathbf{k}) + \hat{H}_{SO} + \hat{H}_B$, with $\mathbf{k} = \tau\mathbf{K} + \mathbf{q}$. Next, we replace $\hat{H}_0(\mathbf{k})$ by the $\mathbf{k}\cdot\mathbf{p}$ Hamiltonian, $\hat{H}_0^{(\mathbf{k}\cdot\mathbf{p})}(\mathbf{k})$, introducing in Eq. (B.7) in **Appendix B**. Since the spin-degree of freedom is irrelevant in $\hat{H}_0^{(\mathbf{k}\cdot\mathbf{p})}(\mathbf{k})$, we only concentrate on the spatial part. By Eq. (2.17), we have the

$$\hat{H}_0^{(\mathbf{k}\cdot\mathbf{p})}(\mathbf{k} = \tau\mathbf{K} + \mathbf{q}) = \begin{pmatrix} \varepsilon_0 + \tau h_x q_x & \tau h_y q_y \\ \tau h_y q_y & \varepsilon_0 - \tau h_x q_x \end{pmatrix} = \varepsilon_0 \hat{\pi}_0 + \tau h \begin{pmatrix} q_x & q_y \\ q_y & -q_x \end{pmatrix}. \quad (3.7)$$

The basis set we employed here is the two degenerate Bloch states exact on $\tau\mathbf{K}$, i.e.

$$\left\{ \left| n, \tau \right\rangle_0 \right\} = \left\{ \left| 1, \tau \right\rangle_0, \left| 2, \tau \right\rangle_0 \right\}.$$

The subscript "0" stresses the states are **q**-dependent, while the eigen-states of $\hat{H}_0^{(\mathbf{k}\cdot\mathbf{p})}(\mathbf{k})$ do depend on **q** with the explicit forms:

$$\begin{aligned} \left| 1, \tau, \mathbf{q} \right\rangle &= \sin\tfrac{\theta_{\mathbf{q}}}{2} \left| 1, \tau \right\rangle_0 - \cos\tfrac{\theta_{\mathbf{q}}}{2} \left| 2, \tau \right\rangle_0 \text{ and} \\ \left| 2, \tau, \mathbf{q} \right\rangle &= \cos\tfrac{\theta_{\mathbf{q}}}{2} \left| 1, \tau \right\rangle_0 + \sin\tfrac{\theta_{\mathbf{q}}}{2} \left| 2, \tau \right\rangle_0 \end{aligned} \quad (3.8)$$

with energies $\varepsilon_1(\mathbf{q}) = \varepsilon_0 - \tau hq$, $\varepsilon_2(\mathbf{q}) = \varepsilon_0 + \tau hq$, and $\tan\theta_{\mathbf{q}} = \frac{q_y}{q_x}$. Thus, the **q**-dependent basis set with spinor is

$$\left\{ \left| n, \tau, \mathbf{q}; \chi \right\rangle \equiv \left| n, \tau, \mathbf{q} \right\rangle \otimes \left| \chi \right\rangle \right\} = \left\{ \left| 1, \tau, \mathbf{q}; \chi_+ \right\rangle, \left| 2, \tau, \mathbf{q}; \chi_- \right\rangle, \left| 1, \tau, \mathbf{q}; \chi_- \right\rangle, \left| 2, \tau, \mathbf{q}; \chi_+ \right\rangle \right\}, \quad (3.9)$$

where $\chi_{\pm}$ are the spin-up and spin-down states along the direction of in-plane magnetic field, $\mathbf{B}_{\parallel}$. With Eq. (3.9), the Hamiltonian in this basis set would be

$$\hat{H}^{(\text{eff})}(\mathbf{k}) = \hat{H}^{(\text{eff})}(\tau\mathbf{K} + \mathbf{q}) = \varepsilon_0 + \begin{pmatrix} -\tau hq + \varepsilon_{\parallel} & -i\lambda_{SO} & \gamma_{\perp}\varepsilon_{\perp} & 0 \\ +i\lambda_{SO} & \tau hq - \varepsilon_{\parallel} & 0 & \gamma_{\perp}\varepsilon_{\perp} \\ \gamma_{\perp}\varepsilon_{\perp} & 0 & -\tau hq + \varepsilon_{\parallel} & -i\lambda_{SO} \\ 0 & \gamma_{\perp}\varepsilon_{\perp} & +i\lambda_{SO} & \tau hq - \varepsilon_{\parallel} \end{pmatrix}. \quad (3.10)$$

Here we define the Zeeman splitting energies by $\hat{H}_{\parallel}\chi_{\pm} = \pm\varepsilon_{\parallel}\chi_{\pm}$, and $\hat{H}_{\perp}\chi_{\pm} = \gamma_{\perp}\varepsilon_{\perp}\chi_{\mp}$, with $\varepsilon_{\parallel} = \frac{1}{2}g\mu_B|\mathbf{B}_{\parallel}| > 0$, while $\varepsilon_{\perp} = \frac{1}{2}g\mu_B|B_{\perp}| > 0$ and $\gamma_{\perp} = \pm 1$ indicating the direction of $\mathbf{B}_{\perp} = B_{\perp}\hat{z} = \gamma_{\perp}|B_{\perp}|\hat{z}$. Thus, it is straightforward to derive the matrix elements

$$\left\langle n,\tau,\mathbf{q};\chi_{\mu}\left|\hat{H}_{\parallel}\right|n',\tau,\mathbf{q};\chi_{\mu'}\right\rangle = \mu\varepsilon_{\parallel}\delta_{n,n'}\delta_{\mu,\mu'} \text{ and}$$
$$\left\langle n,\tau,\mathbf{q};\chi_{\mu}\left|\hat{H}_{\perp}\right|n',\tau,\mathbf{q};\chi_{\mu'}\right\rangle = \varepsilon_{\perp}\delta_{n,n'}\delta_{\mu,\bar{\mu}'}.$$

On the other hand, the matrix elements of $\hat{H}_{\mathrm{SO}}$ are

$$\begin{aligned}\left\langle n,\tau,\mathbf{q};\chi_{\mu}\left|\hat{H}_{\mathrm{SO}}\right|n',\tau,\mathbf{q};\chi_{\mu'}\right\rangle &= \left\langle n,\tau,\mathbf{q};\chi_{\mu}\left|\hat{V}_{\mathrm{SO}}\otimes\hat{\sigma}_z\right|n',\tau,\mathbf{q};\chi_{\mu'}\right\rangle \\ &= \left\langle n,\tau,\mathbf{q}\left|\hat{V}_{\mathrm{SO}}\right|n',\tau,\mathbf{q}\right\rangle\delta_{\mu,\bar{\mu}'}\end{aligned} \tag{3.11}$$

From Eqs. (3.8) and (2.20), we have

$$\left\langle n,\tau;\mathbf{q}\left|\hat{V}_{\mathrm{SO}}\right|n',\tau,\mathbf{q}\right\rangle = -\lambda_{\mathrm{SO}}\hat{\pi}_2.$$

The final form of the effective Hamiltonian in Eq. (3.10) seems independent to *K*- and *K'*- valleys, but remember, the basis set in Eq. (3.9) already carries the valley information, τ.

By Eq. (3.10), we can deduce the energies:

$$\varepsilon_{\eta\xi}(q) = \eta\sqrt{\lambda_{so}^2 + h^2q^2 + \varepsilon_{//}^2 + \varepsilon_{\perp}^2 + 2\xi\sqrt{\lambda_{so}^2\varepsilon_{\perp}^2 + h^2q^2\varepsilon_{//}^2 + \varepsilon_{\perp}^2h^2q^2}} \tag{3.11}$$

with $\eta = \pm 1$ and $\xi = \pm 1$, characterizing the four separated bands, and $H_q^2 = (hq)^2$. At $q = 0$, i.e. exact on $\tau\mathbf{K}$-point, $\varepsilon_{\eta\xi} = \eta\sqrt{(\lambda_{\mathrm{SO}} + \xi\varepsilon_{\perp})^2 + \varepsilon_{\parallel}^2}$, and we find if $\varepsilon_{\perp} = 0$ ($B_{\perp} = 0$), there are two doubly-degenerate energy at $\tau\mathbf{K}$-point.

Fig 3.3 plots the effective theory for the lowest band structures of 2DEG in MTP with SOI and magnetic field about *K*-valley.

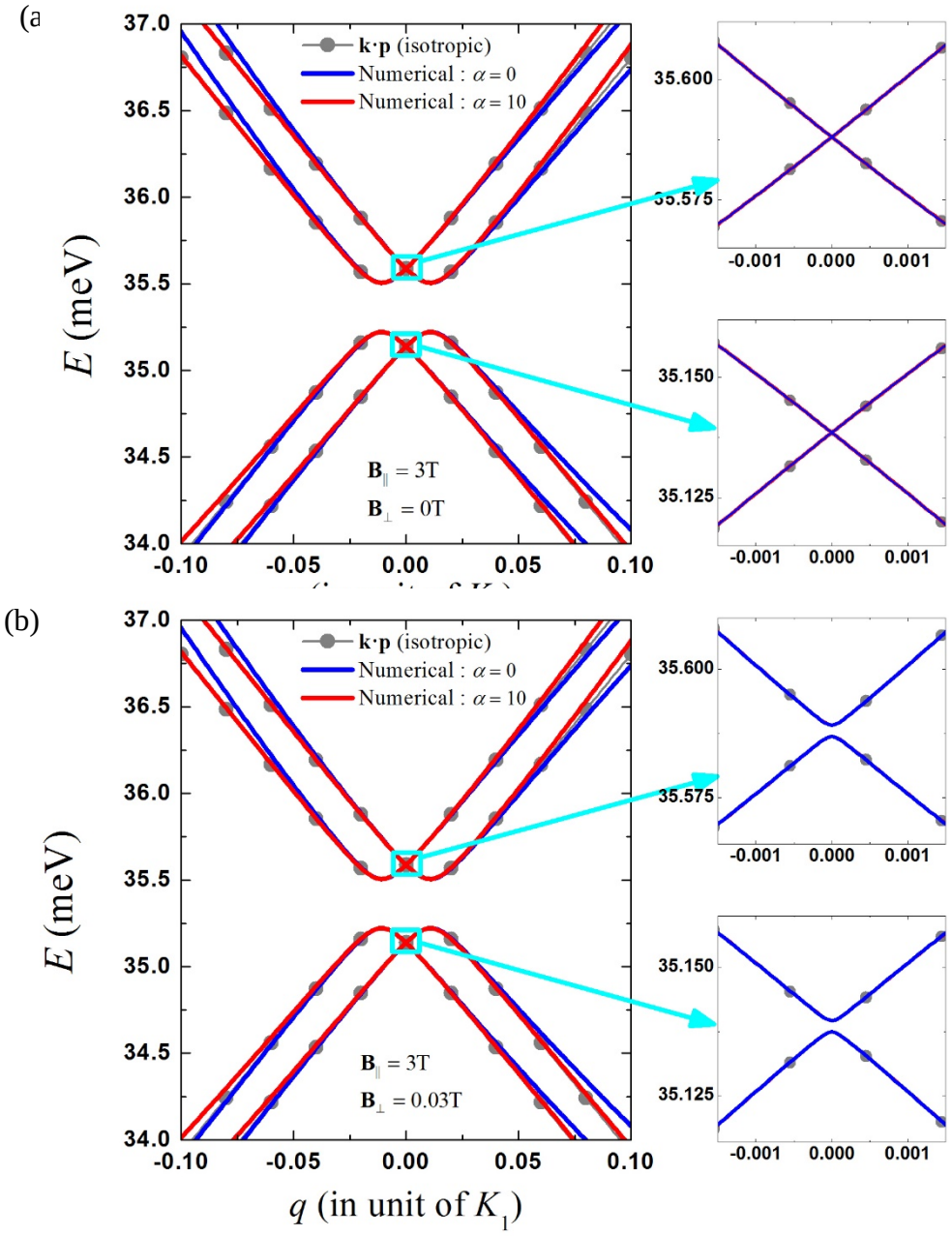

Fig 3.3 The band structures from the effective theory around *K* point. (a) The out-of-plane field, $\mathbf{B}_\perp = 0\text{T}$ and (b) $\mathbf{B}_\perp = 0.03\text{T}$. The solid red and blue lines are those bands from numerical results with different **q**-directions ($\alpha = 0$ and $\alpha = 10$ for blue and red lines, respectively). The parameters we employ here are $m^* = 0.023m_e$; the MTP strength $U_0 = 165\,\text{meV}$ with diameter $d = 0.663a$ and $a = 40\,\text{nm}$ is the lattice constant. The SOI coupling constant is $\lambda = 120\text{Å}^2$

Chapter 4

Topological analysis of the effective theory

The topological feature of the MTP with SOI and magnetic field is analytically discussed in this section via the effective theory introducing in **Sec. 3.3**. In **Sec. 4.1**, a brief but general review of the Berry phase and Berry curvature is presented. Based on these, in **Sec. 4.2**, we can discuss the topological invariants, such as the Chern number and Z2 numbers, which are utilized to classify the topological nature of the system. Finally, based on the effective theory introduced in **Sec. 3.3**, we analytically calculate the Chern numbers of the MTP system with SOI and general magnetic field. These will be shown in **Sec. 4.3**.

4.1 Berry phase and Berry curvature

The Berry phase was proposed in 1984 by Michael Berry. It rises from a quantum system with an external time-dependent parameter $\mathbf{k}(t)$ by denoting it as $H(\mathbf{k}(t))$, following the cyclic adiabatic evolution. When $\mathbf{k}(t)$ moves slowly along a path C, with the n'th eigenenergy being non-degenerate everywhere along the path, and the instantaneous eigenstate $|u_{\mathbf{k}(t),n}\rangle$ satisfies the eigenvalue equation at time t, $H(\mathbf{k}(t))|u_{\mathbf{k}(t),n}\rangle = \varepsilon_n(\mathbf{k}(t))|u_{\mathbf{k}(t),n}\rangle$.
According to the quantum adiabatic theorem, a system initially in one of its eigenstates $|u_{\mathbf{k}(0),n}\rangle$ will stay as an instantaneous eigenstate of $H(\mathbf{k}(t))$ throughout the process. The state at time t can be written as,

$$|\Psi_n(t)\rangle = e^{-i\gamma_n(t)} e^{-\frac{i}{\hbar}\int_0^t \varepsilon_n(\mathbf{k}(t'))dt'} |u_{\mathbf{k}(t),n}\rangle. \tag{4.1}$$

The first exponential term in Eq. (4.1) is geometric phase and the second exponential term is dynamics phase. The extra phase $e^{i\gamma_n(t)}$ is added for each eigen-state. Michael Berry pointed that the geometric phase $e^{i\gamma_n(t)}$ may not return its origin value after the evolution. Hence it is not necessarily removable.
Substitute Eq. (4.1) into the time-dependent Schrödinger equation

$$i\hbar\frac{\partial}{\partial t}|\Psi_n(t)\rangle = H(\mathbf{k}(t))|\Psi_n(t)\rangle,$$

and multiply it from the left by $\langle u_{\mathbf{k}(t),n}|$, $\gamma_n(t)$ can be expressed as

$$\gamma_n(t) = i\int_0^t \left\langle u_{\mathbf{k}(t'),n}\right| \frac{d}{dt'} \left|u_{\mathbf{k}(t'),n}\right\rangle dt' = i\int_{\mathbf{k}(0)}^{\mathbf{k}(t)} \left\langle u_{\mathbf{k},n}\right| \frac{d}{d\mathbf{k}} \left|u_{\mathbf{k},n}\right\rangle d\mathbf{k}. \tag{4.2}$$

In a cyclic evolution through a closed path $C: \mathbf{k}(0) = \mathbf{k}(\mathrm{t})$.
From Stoke's theorem we have,

$$\gamma_n(C) = i\int_C d\mathbf{S}\cdot\nabla_{\mathbf{k}}\times\langle u_{\mathbf{k},n}|\nabla_{\mathbf{k}}u_{\mathbf{k},n}\rangle = \iint_C d\mathbf{S}\cdot\Omega_n(\mathbf{k}), \tag{4.3}$$

and $\gamma_n(C)$ is known as **Berry phase**.

The gauge invariant of Berry phase that makes Berry phase physical and proves it is measurable by interference phenomena. Considering the gauge transformation $|\tilde{u}_{\boldsymbol{k},n}\rangle = e^{i\Lambda(\mathbf{k})}|u_{\boldsymbol{k},n}\rangle$, where $e^{i\Lambda(\mathbf{k})}$ is a $\mathbf{k}$-dependent phase factor. We have $\langle u_{\mathbf{k},n}|\nabla_{\mathbf{k}}u_{\mathbf{k},n}\rangle = i\nabla_{\mathbf{k}}\Lambda(\mathbf{k}) + \langle u_{\mathbf{k},n}|\nabla u_{\mathbf{k},n}\rangle$, substituting into the LHS of Eq. (4.3), the additional term $\nabla_{\mathbf{k}}\times\nabla\Lambda(\mathbf{k}) = 0$. So we have the gauge freedom of multiplying it with an overall phase factor which can be parameter dependent. The Berry is unchanged by such a phase factor, provided the eigenwave function is kept to be a single valued over the path.

Furthermore, the Berry phase is geometrical because it can be written as line integral over a closed path C in the parameter space. This property makes it possible to express Berry phase in terms of local geometrical quantities. Michael Berry show that the Berry phase can be written as the integral of a field, which is known as **Berry curvature**. From Eq. (4.3), the Berry curvature is denoted by $\Omega_n(\mathbf{k})$,

$$\Omega_n(\mathbf{k}) = i\nabla_{\mathbf{k}}\times\langle u_{\mathbf{k},n}|\nabla_{\mathbf{k}}u_{\mathbf{k},n}\rangle. \tag{4.4}$$

Besides the differential form in Eq. (4.4), the Berry curvature can be also written as a summation over the eigenstates,

$$\Omega_n(\mathbf{k}) = i\sum_{n\neq n'}\frac{\langle u_{\mathbf{k},n}|\partial_{k_x}H(\mathbf{k})|u_{\mathbf{k},n'}\rangle\langle u_{\mathbf{k},n'}|\partial_{k_y}H(\mathbf{k})|u_{\mathbf{k},n}\rangle - (x\leftrightarrow y)}{E_{\mathbf{k},n}-E_{\mathbf{k},n'}}\hat{z}. \tag{4.5}$$

There is no differentiation on the eigenstates involved in Eq. (4.5), therefore it can be evaluated under any gauge choice. This is useful for numerical calculations, in which the condition of a smooth phase choice of the eigenstates is not guaranteed in standard diagonalization algorithms. In addition, Eq. (4.5) gives another insight on the origin of the Berry curvature. The adiabatic approximation adopted earlier is crucially a projection operation, i.e., the dynamics of the system is restricted to the *n*th energy level. The Berry curvature can be viewed as the result of the "residual" interaction of those projected-out energy levels.

On the other hand, the Berry phase is like the Aharonov-Bohm phase of a charged particle traversing a loop including a magnetic flux, while Berry curvature is like the magnetic field. The integral of the Berry curvature over the closed surfaces (ex a sphere or torus), is known to be topological and quantized as integers and is also called **Chern number**.

4.2 Chern number and Z_2 number of topological insulator

The Berry phase or the Berry curvature discussed in previous section enable us to study the topology of the energy band structures. By Eq. (4.5), we can define the Berry curvature of the n-th band, $\Omega_n(\mathbf{k})$, with the varying parameter being the crystal momentum, $\mathbf{k}$. Since the crystal momentum is defined on the first Brillouin zone with the closure property, $\mathbf{k}+\mathbf{G}=\mathbf{k}$, the domain of $\Omega_n(\mathbf{k})$ is a close surface (manifold). According to the Chern theorem, the integral of the Berry curvature over a closed manifold is quantized in unit of 2π, which defines the Chern number of the n[th] band

$$C_n = \frac{1}{2\pi}\int_{B.Z.} \Omega_n(\mathbf{k}) d\mathbf{k} \in \mathbb{Z}.$$

The total Chern number defined by summing over all occupied bands, $C = \sum_{n\in \text{valance}} C_n$, is an invariance provided there is a finite gap separating the valance and conduction bands within the whole Brillouin zone. Thus, C is a topological order that characterize the topology of the bands. Historically, Thouless et al utilize Kubo formula to calculate σ_{xy} of a quantum Hall system and recover $\sigma_{xy} = C\, e^2/h$ which explains the robustness of the quantization of σ_{xy}, and provides a topological understanding of quantum Hall effect (QHE). Following this, the field of topological insulator (or topological phase) arises. General speaking, a topological insulator is an insulator with bulk gap, however, the conducting edge states arise at the boundaries if it is connected to other type of insulator. The Chern number categories the classes of topological phase and the topological phase transition is accompanied by a process of gap closing during the varying of parameters in the Hamiltonian. In this sense, the topological phases are robust under perturbation to the Hamiltonian.

Topological quantities are practically significant in characterizing the electrical transport properties in quantum Hall effects of 2DEG. It has been proposed earlier that the quantum Hall (QH) effect is associated with a topological invariant integer known as Chern number. The value of Chern number n, which gives the quantized Hall conductivity for each band $c\frac{e^2}{\hbar}$, is given by the integral of Bloch wave functions over the magnetic Brillouin zone. Since the Hall conductivity does not obey the time-reversal symmetry (TRS), recently people have proposed that the SOI in a single plane of graphene in absence of magnetic field results in TRS quantum spin Hall (QSH) state which has a bulk energy gap and a pair of gapless spin filtered edge states on the boundary. The QSH effect is analogous to QH effect but it doesn't break TRS. The QH states are specified by Chern numbers, while the QSH states are characterized by Z_2 numbers. As TRS rising, for instance, in a 2D model [8] (π-electron tight-binding model with mirror-symmetry about the plane), the perpendicular spin component S_z

is conserved and the spin-up and spin-down have independent Chern integers $C_\uparrow$ and $C_\downarrow$. TRS requires the Chern number $C = C_\uparrow + C_\downarrow$ is equal to zero, distinguish from ordinary insulator and offers a new class of topological invariant which is classified as Z_2 topological order. The Z_2 invariant is shown as

$$\nu = C_\sigma \mod 2.$$

The value $\nu = 0$ is trivial insulator and $\nu = 1$ is topological insulator (QSH insulator).

At the end of this section, we want to discuss the intuitive 2-band model that manifests the topology of the system. The Hamiltonian of the 2-band model is, generally, expressed in the combination of Pauli matrices:

$$\hat{H}(\mathbf{k}) = \mathbf{h}(\mathbf{k}) \cdot \hat{\boldsymbol{\sigma}} = \begin{pmatrix} h_z & h_x - ih_y \\ h_x + ih_y & -h_z \end{pmatrix}$$

The eigen-states are

$$|\mathbf{k}, +\rangle = \begin{pmatrix} \cos\frac{\theta}{2} e^{-i\frac{\varphi}{2}} \\ \sin\frac{\theta}{2} e^{i\frac{\varphi}{2}} \end{pmatrix}, \text{ and } |\mathbf{k}, -\rangle = \begin{pmatrix} \sin\frac{\theta}{2} e^{-i\frac{\varphi}{2}} \\ -\cos\frac{\theta}{2} e^{i\frac{\varphi}{2}} \end{pmatrix},$$

where + and – stand for conduction and valance bands, respectively, and θ, φ are the polar and azimuth angles of the unit vector, $\hat{\boldsymbol{n}} = \|\mathbf{h}\|^{-1}\mathbf{h}(\mathbf{k}) = (\sin\theta\cos\varphi, \sin\theta\sin\varphi, \cos\theta)$, defined over the Bloch sphere. Assume there is an overall gap separating the conduction and valance bands, thus it's straightforward that

$$\partial_\mu |\mathbf{k}, -\rangle = \frac{\partial}{\partial k_\mu} |\mathbf{k}, -\rangle = \frac{1}{2} \begin{pmatrix} \cos\frac{\theta}{2} e^{-i\frac{\varphi}{2}} \partial_\mu\theta - i\sin\theta e^{-i\frac{\varphi}{2}} \partial_\mu\varphi \\ \sin\frac{\theta}{2} e^{i\frac{\varphi}{2}} \partial_\mu\theta - i\cos\theta e^{i\frac{\varphi}{2}} \partial_\mu\varphi \end{pmatrix}$$

Therefore the Berry curvature of the valance band would be

$$\Omega_-(\mathbf{k}) = \frac{1}{2}\sin\theta\left(\partial_1\theta\partial_2\varphi - \partial_2\theta\partial_1\varphi\right)\hat{z},$$

and the Chern number is

$$C = \frac{1}{4\pi}\int_{B.Z.} \sin\theta\left(\partial_1\theta\partial_2\varphi - \partial_2\theta\partial_1\varphi\right) d\mathbf{k} = \frac{1}{4\pi}\int_{B.Z.} \partial_1\hat{\mathbf{n}} \times \partial_2\hat{\mathbf{n}} \cdot \hat{\mathbf{n}} d\mathbf{k} \qquad (4.6)$$

Since $\hat{\mathbf{n}}$ is a unit vector which defines the mapping from Brillouin zone to the normal vector at Bloch sphere, $\hat{\mathbf{n}} \perp \partial_\mu \hat{\mathbf{n}}$; the integrand of Eq. (4.6) immediately interpreted as the solid angle spanned by $\partial_1\hat{\mathbf{n}}dk_x$ and $\partial_2\hat{\mathbf{n}}dk_y$. Integrate over the whole Brillouin zone and the Chern number, here, defines the number of times $\hat{\mathbf{n}}$ wrapping around the Bloch sphere as Brillouin zone mapping to $\hat{\mathbf{n}}$.

4.3 Topological analysis of the effective theory

In this section, the topological quantities such as Berry curvature and Chern (or Z_2) number of the muffin-tin potential lattice with SOI and general magnetic field, B, is discussed. In the former thesis of our group [15], we have demonstrated the successful of effective theory in calculating the Berry curvature and Chern number. Therefore, we will continually employ the effective Hamiltonian in Eq. (3.10) and analytically discuss the band topology.

Particularly, the effective Hamiltonian we considering here is, by Eq. (3.10),

$$\hat{H}^{(\mathrm{eff})}(\tau\mathbf{K}+\mathbf{q}) = \varepsilon_0 + \begin{pmatrix} -\tau hq + \varepsilon_{\parallel} & -i\lambda_{\mathrm{SO}} & \gamma_{\perp}\varepsilon_{\perp} & 0 \\ +i\lambda_{\mathrm{SO}} & \tau hq - \varepsilon_{\parallel} & 0 & \gamma_{\perp}\varepsilon_{\perp} \\ \gamma_{\perp}\varepsilon_{\perp} & 0 & -\tau hq - \varepsilon_{\parallel} & -i\lambda_{\mathrm{SO}} \\ 0 & \gamma_{\perp}\varepsilon_{\perp} & +i\lambda_{\mathrm{SO}} & \tau hq + \varepsilon_{\parallel} \end{pmatrix}. \tag{4.7}$$

The parameter, $\gamma_{\perp} = \pm 1$, indicates the direction of magnetic field, $\mathbf{B} = \boldsymbol{B}_{\parallel} + \gamma_{\perp}|B_{\perp}|\hat{z}$. The basis set is defined in Eqs. (3.8) and (3.9) with $\chi_{\pm}$ denotes the spin-up/-down along $\mathbf{B}_{\parallel}$. Hence, the general eigen solutions of Eq. (4.7) would be

$$\begin{aligned} |\psi(\mathbf{q})\rangle = {} & A(\mathbf{q})|1,\tau,\mathbf{q};\chi_{+}\rangle + B(\mathbf{q})|2,\tau,\mathbf{q};\chi_{-}\rangle \\ + {} & C(\mathbf{q})|1,\tau,\mathbf{q};\chi_{-}\rangle + D(\mathbf{q})|2,\tau,\mathbf{q};\chi_{+}\rangle \end{aligned}, \tag{4.8}$$

and immediately, we have

$$\begin{aligned} \nabla|1,\tau,\mathbf{q};\chi_{\mu}\rangle &= \nabla\left\{\sin\tfrac{\theta_{\mathbf{q}}}{2}|1,\tau\rangle_0 \otimes |\chi_{\mu}\rangle - \cos\tfrac{\theta_{\mathbf{q}}}{2}|2,\tau\rangle_0 \otimes |\chi_{\mu}\rangle\right\} \\ &= \left\{\cos\tfrac{\theta_{\mathbf{q}}}{2}|1,\tau\rangle_0 \otimes |\chi_{\mu}\rangle + \sin\tfrac{\theta_{\mathbf{q}}}{2}|2,\tau\rangle_0 \otimes |\chi_{\mu}\rangle\right\}\tfrac{1}{2}\nabla\theta_{\mathbf{q}} \\ &= |2,\tau,\mathbf{q};\chi_{\mu}\rangle\tfrac{1}{2}\nabla\theta_{\mathbf{q}} \text{ and} \end{aligned} \tag{4.9a}$$

$$\begin{aligned} \nabla|2,\tau,\mathbf{q};\chi_{\mu}\rangle &= \nabla\left\{\cos\tfrac{\theta_{\mathbf{q}}}{2}|1,\tau\rangle_0 \otimes |\chi_{\mu}\rangle + \sin\tfrac{\theta_{\mathbf{q}}}{2}|2,\tau\rangle_0 \otimes |\chi_{\mu}\rangle\right\} \\ &= \left\{-\sin\tfrac{\theta_{\mathbf{q}}}{2}|1,\tau\rangle_0 \otimes |\chi_{\mu}\rangle + \cos\tfrac{\theta_{\mathbf{q}}}{2}|2,\tau\rangle_0 \otimes |\chi_{\mu}\rangle\right\}\tfrac{1}{2}\nabla\theta_{\mathbf{q}} \\ &= -|1,\tau,\mathbf{q};\chi_{\mu}\rangle\tfrac{1}{2}\nabla\theta_{\mathbf{q}}, \end{aligned} \tag{4.9b}$$

which is useful in calculating

$$\langle\psi|\nabla|\psi\rangle = \begin{Bmatrix} A^*\langle 1,\tau,\mathbf{q};\chi_+|+ \\ B^*\langle 2,\tau,\mathbf{q};\chi_-|+ \\ C^*\langle 1,\tau,\mathbf{q};\chi_-|+ \\ D^*\langle 2,\tau,\mathbf{q};\chi_+| \end{Bmatrix} \begin{Bmatrix} (\nabla A)|1,\tau,\mathbf{q};\chi_+\rangle + \frac{1}{2}(\nabla\theta_{\mathbf{q}})A|2,\tau,\mathbf{q};\chi_+\rangle + \\ (\nabla B)|2,\tau,\mathbf{q};\chi_-\rangle - \frac{1}{2}(\nabla\theta_{\mathbf{q}})B|1,\tau,\mathbf{q};\chi_-\rangle + \\ (\nabla C)|1,\tau,\mathbf{q};\chi_-\rangle + \frac{1}{2}(\nabla\theta_{\mathbf{q}})C|2,\tau,\mathbf{q};\chi_-\rangle + \\ (\nabla D)|2,\tau,\mathbf{q};\chi_+\rangle - \frac{1}{2}(\nabla\theta_{\mathbf{q}})D|1,\tau,\mathbf{q};\chi_+\rangle \end{Bmatrix} \quad (4.10)$$

$$= \begin{Bmatrix} A^*\nabla A - \frac{1}{2}(\nabla\theta_{\mathbf{q}})A^*D + B^*\nabla B + \frac{1}{2}(\nabla\theta_{\mathbf{q}})B^*C + \\ C^*\nabla C - \frac{1}{2}(\nabla\theta_{\mathbf{q}})C^*B + D^*\nabla D + \frac{1}{2}(\nabla\theta_{\mathbf{q}})D^*A \end{Bmatrix}.$$

From Eq. (4.10) and the definition of Berry curvature in Eq. (4.4), we have

$$\begin{aligned} \Omega_{n,\tau}(\mathbf{q}) &= i\,\nabla\times\langle\psi_{n,\tau}(\mathbf{q})|\nabla|\psi_{n,\tau}(\mathbf{q})\rangle \\ &= i\,\nabla\times\begin{Bmatrix} A^*_{n,\tau}\nabla A_{n,\tau} - \frac{1}{2}(\nabla\theta_{\mathbf{q}})A^*_{n,\tau}D_{n,\tau} + B^*_{n,\tau}\nabla B_{n,\tau} + \frac{1}{2}(\nabla\theta_{\mathbf{q}})B^*_{n,\tau}C_{n,\tau} + \\ C^*_{n,\tau}\nabla C_{n,\tau} - \frac{1}{2}(\nabla\theta_{\mathbf{q}})C^*_{n,\tau}B_{n,\tau} + D^*_{n,\tau}\nabla D_{n,\tau} + \frac{1}{2}(\nabla\theta_{\mathbf{q}})D^*_{n,\tau}A_{n,\tau} \end{Bmatrix} \\ &= i\,\tfrac{1}{2}\nabla\times\left\{(\nabla\theta_{\mathbf{q}})\left(D^*_{n,\tau}A_{n,\tau} - A^*_{n,\tau}D_{n,\tau} + B^*_{n,\tau}C_{n,\tau} - C^*_{n,\tau}B_{n,\tau}\right)\right\} \end{aligned} \quad (4.11)$$

In the final step of Eq. (4.11), terms like $\nabla\times A^*\nabla A$, for example, is dropped because

$$\begin{aligned} \nabla\times\left(A^*\nabla A\right) &= \nabla A^*\times\nabla A + \cancel{A^*\nabla\times\nabla A} \\ &= (\nabla A_R - i\,\nabla A_I)\times(\nabla A_R + i\,\nabla A_I) \\ &= 2i\,\nabla A_R\times\nabla A_I = 0. \end{aligned}$$

Here, $A_R(q)$and $A_I(q)$, are functions of q since the Hamiltonian in Eq. (3.10) depends on q only. Accordingly, both ∇A_R and ∇A_I are parallel to $\mathbf{q}$ resulting in null of $\nabla A_R\times\nabla A_I$. Finally, we define

$$F_{n,\tau}(\mathbf{q}) = D^*_{n,\tau}A_{n,\tau} - A^*_{n,\tau}D_{n,\tau} + B^*_{n,\tau}C_{n,\tau} - C^*_{n,\tau}B_{n,\tau}, \quad (4.12)$$

and the Berry curvature in Eq. (4.11) is further reduced

$$\begin{aligned} \Omega_{n,\tau}(\mathbf{q}) &= i\,\nabla\times\langle\psi_{n,\tau}(\mathbf{q})|\nabla|\psi_{n,\tau}(\mathbf{q})\rangle \\ &= i\,\tfrac{1}{2}\nabla\times\left\{(\nabla\theta_{\mathbf{q}})\left(D^*_{n,\tau}A_{n,\tau} - A^*_{n,\tau}D_{n,\tau} + B^*_{n,\tau}C_{n,\tau} - C^*_{n,\tau}B_{n,\tau}\right)\right\} \\ &= i\,\tfrac{1}{2}\nabla\times\left\{(\nabla\theta_{\mathbf{q}})F_{n,\tau}(\mathbf{q})\right\} = i\,\tfrac{1}{2}\left\{\nabla F_{n,\tau}(\mathbf{q})\right\}\times\nabla\theta_{\mathbf{q}}. \end{aligned} \quad (4.13)$$

The gradient of the angle, $\theta_{\mathbf{q}} = \tan^{-1}(q_y/q_x)$, is

$$\begin{aligned} \nabla\theta_{\mathbf{q},\tau} &= \tfrac{\partial}{\partial q_x}\tan^{-1}\tfrac{q_y}{q_x}\,\hat{x} + \tfrac{\partial}{\partial q_y}\tan^{-1}\tfrac{q_y}{q_x}\,\hat{y} \\ &= \left(\sec\theta_{\mathbf{q}}\right)^{-2}\left(\tfrac{\partial}{\partial q_x}\tfrac{q_y}{q_x}\,\hat{x} + \tfrac{\partial}{\partial q_y}\tfrac{q_y}{q_x}\,\hat{y}\right) \\ &= \tfrac{q_x^2}{q^2}\left(-\tfrac{q_y}{q_x^2}\,\hat{x} + \tfrac{1}{q_x}\,\hat{y}\right) = \tfrac{1}{q^2}\left(-q_y\,\hat{x} + q_x\,\hat{y}\right) \end{aligned}$$

The Chern number is straightforwardly,

$$
\begin{aligned}
C_n &= \tfrac{1}{2\pi}\int \Omega_n(\boldsymbol{q})\cdot\hat{z}d^2q \\
&= \tfrac{i}{4\pi}\int \left\{\nabla F_{n,\tau}(\boldsymbol{q})\right\}\times\nabla\theta_{\boldsymbol{q}}\cdot\hat{z}d^2q \\
&= \tfrac{i}{4\pi}\int \left\{\tfrac{\partial}{\partial q}F_{n,\tau}(q)\right\}\tfrac{1}{q}(q_x\hat{x}+q_y\hat{y})\times\tfrac{1}{q^2}(-q_y\hat{x}+q_x\hat{y})\cdot\hat{z}d^2q \\
&= \tfrac{i}{4\pi}\int \left\{\tfrac{\partial}{\partial q}F_{n,\tau}(q)\right\}\tfrac{1}{q^3}q^2\hat{z}\cdot\hat{z}\left(2\pi q\right)dq \\
&= \tfrac{i}{2}\int \tfrac{\partial}{\partial q}F_{n,\tau}(q)dq = \tfrac{i}{2}\Big[F_{n,\tau}(q)\Big]_{q=0}^{q=\infty} = -\tfrac{i}{2}F_{n,\tau}(q=0)
\end{aligned}
\tag{4.14}
$$

Therefore, the Chern number is determined by the function, $F_{n,\tau}(q)$, at $q=0$ and $q=\infty$. These values are derived in **Appendix F** with the simple results $F_{n,\tau}(\infty)=0$ and $F_{n,\tau}(0)=-i\xi\gamma_\perp$. Note that at $q=0$, the Hamiltonian in Eq. (4.7) is automatically valley-independent, therefore, it concludes the Chern number, C_n, is also τ-independent. Finally, the Chern number of the band label by η and ξ is

$$
C_{\eta\xi} = -\frac{1}{2}\xi\gamma_\perp \tag{4.15}
$$

For the special case of $\mathbf{B}_\perp = 0$, the effective Hamiltonian in Eq. (4.7) becomes

$$
\hat{H}^{(\mathrm{eff})}(\tau\mathbf{K}+\mathbf{q}) = \varepsilon_0 + \begin{pmatrix} -\tau hq+\varepsilon_\parallel & -i\lambda_{\mathrm{SO}} & 0 & 0 \\ +i\lambda_{\mathrm{SO}} & \tau hq-\varepsilon_\parallel & 0 & 0 \\ 0 & 0 & -\tau hq-\varepsilon_\parallel & -i\lambda_{\mathrm{SO}} \\ 0 & 0 & +i\lambda_{\mathrm{SO}} & \tau hq+\varepsilon_\parallel \end{pmatrix} \tag{4.16}
$$

which is decomposed into two uncoupled 2×2 matrices. Therefore the general eigen states of Eq. (4.16) would be

$$
\begin{aligned}
\left|\psi(\mathbf{q})\right\rangle &= A(\mathbf{q})\left|1,\tau,\mathbf{q};\chi_+\right\rangle + B(\mathbf{q})\left|2,\tau,\mathbf{q};\chi_-\right\rangle, \text{ or} \\
\left|\psi(\mathbf{q})\right\rangle &= C(\mathbf{q})\left|1,\tau,\mathbf{q};\chi_-\right\rangle + D(\mathbf{q})\left|2,\tau,\mathbf{q};\chi_+\right\rangle
\end{aligned}
$$

Following similar derivation from Eq. (4.10) to Eq. (4.11), it is easy to show the Chern numbers here are zero for all the four bands.

In conclusion, we have derived the Chern numbers that manifest the band topology of the MTP system. The Chern numbers are characterized by the parameters $\gamma_\perp\varepsilon_\perp$ which are introduced in Eq. (4.7). If only in-plane magnetic field is presence (i.e. $\varepsilon_\perp = 0$), the Chern numbers are zero, independent of the magnitude and direction of $\mathbf{B}_\parallel$. However, for the presence of both $\mathbf{B}_\parallel$ and $\mathbf{B}_\perp$, the Chern numbers become $\frac{1}{2}\xi\gamma_\perp$, depending on the direction of $\mathbf{B}_\perp$ (still independent of the magnitude of magnetic field). **Fig** 4.1 (a), (b), (c) and (d) label the Chern numbers for the lower bands under the different conditions of magnetic field.

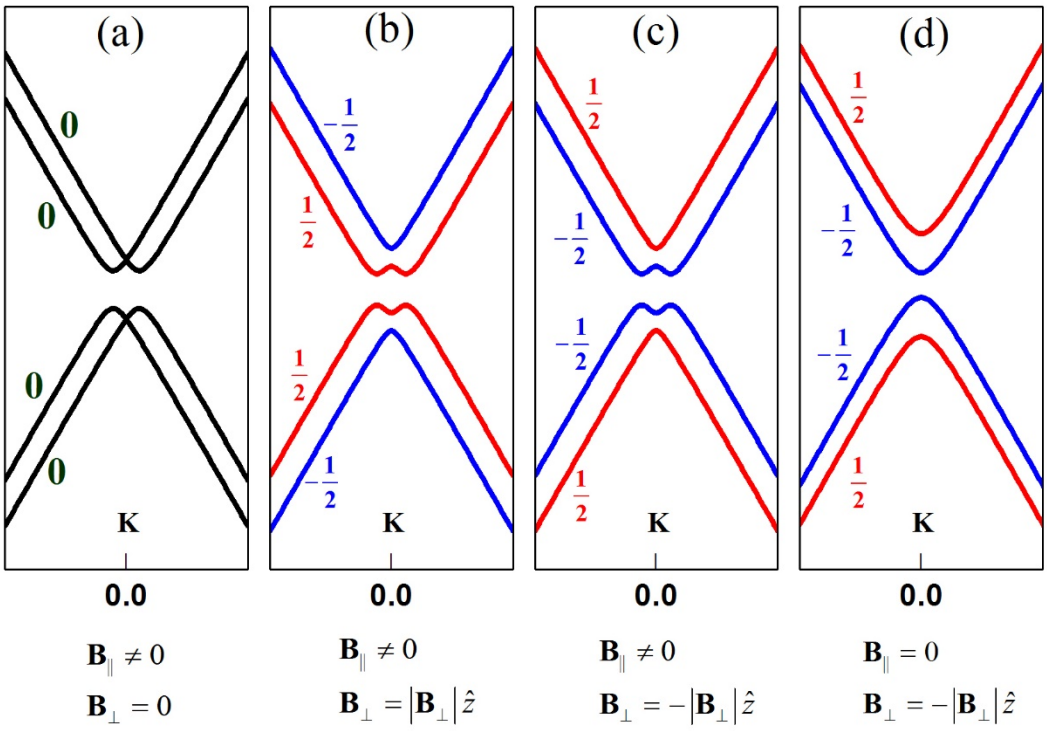

Fig 4.1 The Chern numbers of the lowest 4 bands near the *K* point. (a) $\mathbf{B}_{\parallel} \neq 0, \mathbf{B}_{\perp} = 0$ (b) $\mathbf{B}_{\parallel} \neq 0, \mathbf{B}_{\perp} = |\mathbf{B}_{\perp}|\hat{z}$ (c) $\mathbf{B}_{\parallel} \neq 0, \mathbf{B}_{\perp} = -|\mathbf{B}_{\perp}|\hat{z}$ (d) $\mathbf{B}_{\parallel} = 0, \mathbf{B}_{\perp} = -|\mathbf{B}_{\perp}|\hat{z}$. The Chern numbers of the band are indicated by the numbers with corresponding color. The SOI are present for all of them. The parameters we employ here are $m^* = 0.023m_e$; the MTP strength $U_0 = 165\text{meV}$ with diameter, $d = 0.663a$, where $a = 40\,\text{nm}$ is the lattice constant. The SOI coupling constant is $\lambda = 120\text{Å}^2$.

Chapter 5

Conclusion and future work

The Chern numbers for the MTP lattice with SOI and magnetic field is analytically derived. From Fig. 4.1, the Z_2 nature of the system is robustness under external magnetic field. For the presence of only in-plane magnetic field, the spin-up and spin-down states along *z*-direction are no more good quantum states. The mixing of these spin bands results in null Chern numbers meaning the breaking of topological feature. However, with arbitrary small out-of-plane magnetic field, the Z_2 nature is restored. These conclude the robustness of the topological properties of 2DEG subjected to MTP with SOI.

The existence of helical edge states is expected for a Z_2 topological insulator. However, base on the effective Hamiltonian, we failed in the searching of these edge states. On the other hand, lessons from graphene with SOI, although the effective Hamiltonian predicts the correct Chern numbers (comparing with the full tight-binding Hamiltonian), the finding edge states is out of the scope of effective Hamiltonian. Therefore, the extension work of this thesis is resuming the searching of edge states via the full Hamiltonian.

Appendix A

The Fourier transform of the MTP

In this appendix, we show the derivation of coefficient $\tilde{V}_m$ in Eq. (2.3). The 2DEG is modulated by a two-dimensional MTP in the explicit potential form

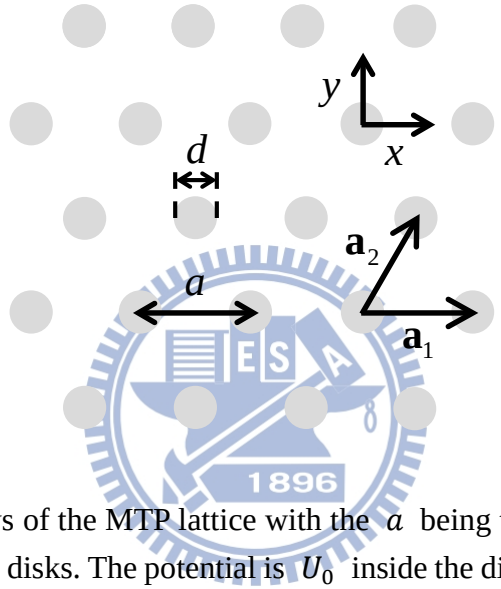

Fig A.1 : The top views of the MTP lattice with the a being the distance between the centers of two adjacent disks. The potential is U_0 inside the disk with diameter d and zero outside.

$$
\begin{aligned}
&V(\mathbf{r}) = \textstyle\sum_{i,j} \tilde{V}\left(\mathbf{r} - \mathbf{R}_{ij}\right) \\
&= \textstyle\sum_{i,j=-\infty}^{\infty} \tilde{V}\left(\mathbf{r} - 2\pi i\frac{\mathbf{a}_1}{2\pi} - 2\pi j\frac{\mathbf{a}_2}{2\pi}\right) \\
&= \textstyle\sum_{i,j=-\infty}^{\infty} \tilde{V}\left(\mathbf{r} - \tau_1\frac{\mathbf{a}_1}{2\pi} - \tau_2\frac{\mathbf{a}_2}{2\pi}\right) \\
&= \textstyle\sum_{i,j=-\infty}^{\infty} \tilde{V}(2\pi i, 2\pi j, \mathbf{r}) \\
&= \textstyle\sum_{i,j=-\infty}^{\infty} \tilde{V}(\tau_1, \tau_2, \mathbf{r})
\end{aligned}
\qquad \text{(A.1)}
$$

where $\mathbf{R}_{ij} = i\mathbf{a}_1 + j\mathbf{a}_2$ ($\mathbf{a}_1, \mathbf{a}_2$ are the basis vectors in real space (**Fig** A.1)). Then we use Poisson sum formula (Eq. (A.2)) cast the real-space infinite sum into the reciprocal-space sum.

$$\textstyle\sum_{i=-\infty}^{\infty} f(2\pi i) = \frac{1}{2\pi}\sum_{v=-\infty}^{\infty} F(v)$$

$$F(v) = \textstyle\int_{-\infty}^{\infty} f(\tau)\, e^{iv\tau} d\tau \qquad \text{(A.2)}$$

Therefore, we obtain the expression of periodic potential

$$V(\mathbf{r}) = \frac{1}{2\pi}\sum_{\upsilon_1=-\infty}^{\infty}\int_{-\infty}^{\infty}\frac{1}{2\pi}\sum_{\upsilon_2=-\infty}^{\infty}\int_{-\infty}^{\infty}\tilde{V}(\tau_1,\tau_2,\mathbf{r})e^{-i\upsilon_1\tau_1}d\tau_1 e^{-i\upsilon_2\tau_2}d\tau_2$$

$$= \left(\frac{1}{2\pi}\right)^2\sum_{\upsilon_1=-\infty}^{\infty}\sum_{\upsilon_2=-\infty}^{\infty}\int_{-\infty}^{\infty}\tilde{V}\left(\mathbf{r}-\tau_1\frac{\mathbf{a}_1}{2\pi}-\tau_2\frac{\mathbf{a}_2}{2\pi}\right)e^{-i\upsilon_1\tau_1}d\tau_1 e^{-i\upsilon_2\tau_2}d\tau_2 \quad (A.3)$$

where $\mathbf{b_1}=2\pi\frac{\mathbf{a}_2\times\hat{z}}{(\mathbf{a}_1\times\mathbf{a}_2)}$, $\mathbf{b_2}=2\pi\frac{\hat{z}\times\mathbf{a}_1}{(\mathbf{a}_1\times\mathbf{a}_2)}$,
$\mathbf{b_1}\cdot\mathbf{a}_1 = 2\pi, \mathbf{b_1}\cdot\mathbf{a}_2 = \mathbf{0};\ \mathbf{b_2}\cdot\mathbf{a}_2 = 2\pi, \mathbf{b_2}\cdot\mathbf{a}_1 = \mathbf{0}$, so
$\mathbf{v} = \sum_{\gamma}^{\mathbf{2}}\upsilon_{\boldsymbol{\gamma}}\mathbf{b}_\gamma;\ \boldsymbol{\tau} = \sum_{\gamma}^{2}\tau_\gamma\,\mathrm{a}_\gamma;\ \mathbf{v}\cdot\boldsymbol{\tau} = 2\pi\sum_{\gamma}^{2}\upsilon_\gamma\tau_\gamma,$ (A.4)

where $\mathbf{v}$ is the vector in $\mathbf{k}$-space ($\mathbf{b}_\gamma$ is the basis vector in $\mathbf{k}$-space); $\boldsymbol{\tau}$ is the real-space vector, and υ_γ, τ_γ are the coefficients for those basis vectors, then we substitute Eq. (A.4) into Eq. (A.3) and obtain the integral term

$$\int V\left(\mathbf{r}-\tfrac{\tau}{2\pi}\right)e^{-i\frac{(\mathbf{v}\cdot\boldsymbol{\tau})}{2\pi}}d\tau_1 d\tau_2$$

$$= (2\pi)^2\int\tilde{V}\,(\boldsymbol{\tau}')e^{-i\frac{\mathbf{v}(\mathbf{r}-\boldsymbol{\tau}')}{2\pi}}d\tau_1' d\tau_2'$$

$$= \frac{(2\pi)^2}{a_1a_2\sin60^\circ}e^{-i\mathbf{v}\cdot\mathbf{r}}\int\tilde{V}\,(\boldsymbol{\tau})e^{i\mathbf{v}\cdot\boldsymbol{\tau}}d\boldsymbol{\tau} \quad (A.5)$$

where we use $\boldsymbol{\tau}' = \mathbf{r}-\frac{\boldsymbol{\tau}}{2\pi}$ in second row in Eq. (3.5), and the integral term in above equation is

$$e^{-i\mathbf{v}\cdot\mathbf{r}}\int\tilde{V}\,(\boldsymbol{\tau})e^{i\mathbf{v}\cdot\boldsymbol{\tau}}d\boldsymbol{\tau}$$

$$= U_0\int_0^{\frac{d}{2}}e^{i\upsilon\tau\cos\phi}\tau d\phi d\tau = U_0\int_0^{\frac{\upsilon d}{2}}\int_0^{2\pi}e^{ix\cos\phi}\frac{x}{\upsilon}d\phi\frac{1}{\upsilon}dx$$

$$= U_0\left(\tfrac{1}{\upsilon}\right)^2\int_0^{\frac{\upsilon d}{2}}\int_0^{2\pi}\sum_{-\infty}^{\infty}(i)^nJ_n\,(x)e^{in\phi}xd\phi dx$$

$$= U_0\left(\tfrac{1}{\upsilon}\right)^2\int_0^{\frac{\upsilon d}{2}}2\pi J_0(x)xdx = 2\pi U_0\left(\tfrac{1}{\upsilon}\right)^2xJ_1(x)\Big|_0^{\frac{\upsilon d}{2}} = \frac{\pi U_0 d}{\upsilon}J_1\left(\frac{\upsilon d}{2}\right), \quad (A.6)$$

then we substitute Eq. (A.6) into Eq. (A.5) to rewrite Eq. (A.3) in the form of

$$V(\mathbf{r}) = \sum_{i,j}^{\infty}\tilde{V}\left(\mathbf{r}-\mathbf{R}_{ij}\right) = \left(\tfrac{1}{2\pi}\right)^2\frac{(2\pi)^2}{a_1a_2\sin60^\circ}\left(\sum_{\upsilon_1=-\infty}^{\infty}\sum_{\upsilon_2=-\infty}^{\infty}e^{-i\mathbf{v}\cdot\mathbf{r}}\frac{\pi U_0 d}{\upsilon}J_1\left(\frac{\upsilon d}{2}\right)\right)$$

$$= \sum_{\upsilon_1,\upsilon_2=-\infty}^{\infty}e^{i\mathbf{v}\cdot\mathbf{r}}\frac{2\pi U_0 d}{\sqrt{3}\upsilon a_1a_2}J_1\left(\tfrac{\upsilon d}{2}\right) = \sum_m e^{i\mathbf{G}_m\cdot\mathbf{r}}\tilde{V}_m \quad (A.7)$$

where $\mathbf{G}_m = \mathbf{v}$, and the coefficient $\tilde{V}_m = \frac{2\pi U_0 d}{\sqrt{3}|\mathbf{G}_m|a_1a_2}J_1\left(\frac{|\mathbf{G}_m|d}{2}\right)$

Appendix B

Matrix elements of $\mathbf{k}\cdot\mathbf{p}$ theory

In this appendix, we analytically derive the matrix elements of the $\mathbf{k}\cdot\mathbf{p}$ Hamiltonian. Before proceeding, the basis set and its properties is discussed. The basis set, we employ here, is

$$\left\{\left|n,\tau;\mu\right\rangle \equiv \left|n,\tau\right\rangle \otimes \left|\chi_\mu\right\rangle\right\} = \left\{\left|1,\tau;+\right\rangle,\left|2,\tau;+\right\rangle,\left|1,\tau;-\right\rangle,\left|2,\tau;-\right\rangle\right\},$$

where $\{|1,\tau\rangle,|2,\tau\rangle\}$ are the lowest two degenerate states of $\hat{H}_0(\tau\mathbf{K}) = \frac{|\hbar\tau\mathbf{K}+\hat{\mathbf{p}}|^2}{2m^*} + V(\mathbf{r})$ and $\left|\chi_\mu\right\rangle$ is the spin state with +/− labeling spin-up/-down. In the plane-wave basis representation, we have

$$\left\langle \mathbf{r}\middle|n,\tau\right\rangle = e^{i\tau\mathbf{K}\cdot\mathbf{r}}\sum_m C_m^{(n,\tau)} e^{i\mathbf{G}_m\cdot\mathbf{r}}\text{ , and} \tag{B.1}$$

$$\sum_{m'}\left\{\frac{\hbar^2}{2m^*}\left|\tau\mathbf{K}+\mathbf{G}_m\right|^2\delta_{m,m'}+\tilde{V}_{m-m'}\right\}C_{m'}^{(n,\tau)} = \sum_{m'}\left[\hat{H}_0(\tau\mathbf{K})\right]_{m,m'}C_m^{(n,\tau)} = \varepsilon_{n,\tau}C_m^{(n,\tau)}. \tag{B.2}$$

First of all, the coefficients, $C_m^{(n,\tau)}$, are all real since $\hat{H}_0(\tau\mathbf{K})$ is a real symmetric matrix in the plane-wave representation ($\tilde{V}_m \in \mathbb{R}$ for MTP with origin at the inversion center). In addition, from Eqs. (B.1) and (B.2), there're transformations

$$\left[\hat{H}_0(\tau\mathbf{K})\right]_{m,m'} = \left[\hat{H}_0(\bar{\tau}\mathbf{K})\right]_{\bar{m},\bar{m}'}$$

and

$$C_m^{(n,\tau)} = C_{\bar{m}}^{(n,\bar{\tau})} \tag{B.3}$$

connecting the wave-functions and Hamiltonians at different valleys ($\tilde{V}_m = \tilde{V}_{\bar{m}}$ has been employed implicitly). With these understandings in mind, by Eq. (2.14b), we are ready to derive the matrix elements of $\mathbf{k}\cdot\mathbf{p}$ Hamiltonian,

$$\left\langle n,\tau;\mu\middle|\hat{H}_0(\tau\mathbf{K})+\hat{H}_{\mathbf{q}}(\tau\mathbf{K})\cdot\mathbf{q}+\hat{H}_{\mathrm{SO}}(\tau\mathbf{K})\middle|n',\tau;\mu'\right\rangle. \tag{B.4}$$

The first term is straightforward,

$$\left\langle n,\tau;\mu\middle|\hat{H}_0(\tau\mathbf{K})\middle|n',\tau,\mu'\right\rangle = \varepsilon_0\delta_{n,n'}\delta_{\mu,\mu'} = \varepsilon_0\hat{\pi}_0\otimes\hat{\sigma}_0, \tag{B.5}$$

since these bases are degenerate eigen-states of $\hat{H}_0(\tau\mathbf{K})$ with energy ε_0. Here, π_0 and $\{\pi_x,\pi_y,\pi_z\}$ are the 2×2 identity and Pauli matrices for the space spanned by $\{|1,\tau\rangle,|2,\tau\rangle\}$, alone with σ_0 and $\{\sigma_x,\sigma_y,\sigma_z\}$ being those matrices for the spin degrees of freedom. The next term, can be separated into two terms, each of them following different symmetry relations:

$$
\begin{aligned}
&\left\langle n,\tau;\mu\left|\hat{H}_{\mathbf{q}}(\tau\mathbf{K})\cdot\hat{x}q_x\right|n',\tau;\mu'\right\rangle \\
&\quad=\tfrac{\hbar}{m^*}\delta_{\mu,\mu'}\sum_m C_m^{(n,\tau)*}C_m^{(n',\tau)}\left(\hbar\tau\mathbf{K}+\mathbf{G}_m\right)\cdot\hat{x}q_x \\
&\quad=\tfrac{\hbar}{m^*}\delta_{\mu,\mu'}\delta_{n,n'}\sum_m\left|C_m^{(n,\tau)}\right|^2\left(\hbar\tau\mathbf{K}+\mathbf{G}_m\right)\cdot\hat{x}q_x \\
&\quad=\tfrac{\hbar}{m^*}\delta_{\mu,\mu'}\delta_{n,n'}\tau\sum_m\left|C_m^{(n,\tau)}\right|^2\left(\hbar\mathbf{K}+\tau\mathbf{G}_m\right)\cdot\hat{x}q_x \\
&\quad=\tfrac{\hbar}{m^*}\delta_{\mu,\mu'}\delta_{n,n'}\tau\sum_m\left|C_{\bar{m}}^{(n,\bar{\tau})}\right|^2\left(\hbar\mathbf{K}+\bar{\tau}\mathbf{G}_{\bar{m}}\right)\cdot\hat{x}q_x \\
&\quad=q_x\left(h_0\hat{\pi}_0+h_3\hat{\pi}_3\right)\otimes\hat{\sigma}_0
\end{aligned}
\tag{B.6a}
$$

$$
\begin{aligned}
&\left\langle n,\tau;\mu\left|\hat{H}_{\mathbf{q}}(\tau\mathbf{K})\cdot\hat{y}q_y\right|n',\tau;\mu'\right\rangle \\
&\quad=\tfrac{\hbar}{m^*}\delta_{\mu,\mu'}\sum_m C_m^{(n,\tau)*}C_m^{(n',\tau)}\mathbf{G}_m\cdot\hat{y}q_y \\
&\quad=\tfrac{\hbar}{m^*}\delta_{\mu,\mu'}\delta_{n,\bar{n}}\tau\sum_m C_m^{(n,\tau)*}C_m^{(\bar{n},\tau)}\tau\mathbf{G}_m\cdot\hat{y}q_y \\
&\quad=\tfrac{\hbar}{m^*}\delta_{\mu,\mu'}\delta_{n,\bar{n}}\tau\sum_m C_{\bar{m}}^{(n,\bar{\tau})*}C_{\bar{m}}^{(\bar{n},\bar{\tau})}\bar{\tau}\mathbf{G}_{\bar{m}}\cdot\hat{y}q_y \\
&\quad=q_y\left(h_1\hat{\pi}_x+h_2\hat{\pi}_y\right)\otimes\hat{\sigma}_0=q_yh_1\hat{\pi}_x\otimes\hat{\sigma}_0
\end{aligned}
\tag{B.6b}
$$

As shown in **Sec.** 2.3, the symmetry relation of the states, $\{|1,\tau\rangle,|2,\tau\rangle\}$, is employed, resulting in the Kronecker delta factors, $\delta_{n,n'}$ and $\delta_{n,\bar{n}'}$, in Eqs. (B.6a) and (B.6b), respectively. Besides, the τ-dependence in Eq. (B.6) is extracted out of the summation and by Eq. (B.3) along with $\mathbf{G}_{\bar{m}}=-\mathbf{G}_m$, the summand is independent of τ. After that, the π-matrices are utilized to expand the matrix elements with the coefficients, h_i, which are all proportional to τ. Since all the coefficients, $C_m^{(n,\tau)}$, are real, we immediately have $h_2=0$. Finally, as shown in **Sec.** 2.3, h_0 is required to be null and $|h_1|=|h_3|$ in order to be consistent with C_3-rotation symmetry of the energy dispersion. Combined with Eq. (B.5), we have,

$$
\begin{aligned}
\left\langle n,\tau;\mu\left|\hat{H}_0^{(\mathbf{k}\cdot\mathbf{p})}(\mathbf{k})\right|n',\tau;\mu'\right\rangle&=\left\langle n,\tau;\mu\left|\hat{H}_0(\tau\mathbf{K})+\hat{H}_{\mathbf{q}}(\tau\mathbf{K})\cdot\mathbf{q}\right|n',\tau;\mu'\right\rangle \\
&=\left\{\begin{pmatrix}\varepsilon_0 & 0\\ 0 & \varepsilon_0\end{pmatrix}+\tau\begin{pmatrix}h_xq_x & h_yq_y\\ h_yq_y & -h_xq_x\end{pmatrix}\right\}\otimes\hat{\sigma}_0
\end{aligned}
\tag{B.7}
$$

with $\tau h_x=h_3$, $\tau h_y=h_1$, and $|h_x|=|h_y|$. Here, h_x and h_y are the τ-independent constants

The last term in Eq. (B.4) is

$$\begin{aligned}\left\langle n,\tau;\mu\left|\hat{H}_{\mathrm{SO}}(\tau\mathbf{K})\right|n',\tau;\mu'\right\rangle &= -\tfrac{\lambda}{\hbar}\left\langle n,\tau;\mu\left|\boldsymbol{\sigma}\cdot\left(\nabla V\times\mathbf{p}\right)\right|n',\tau;\mu'\right\rangle \\ &= -i\tfrac{\lambda}{\hbar}\sum_{m,m'}C_{m}^{(n,\tau)*}C_{m'}^{(n',\tau)}\tilde{V}_{m-m'}\left(\mathbf{G}_{m-m'}\times\hbar\mathbf{G}_{m'}\right)_{z}\otimes\hat{\sigma}_{z} \\ &= -i\tfrac{\lambda}{\hbar}\sum_{m,m'}C_{\bar{m}}^{(n,\bar{\tau})*}C_{\bar{m}'}^{(n',\bar{\tau})}\tilde{V}_{\bar{m}-\bar{m}'}\left(\mathbf{G}_{\bar{m}-\bar{m}'}\times\hbar\mathbf{G}_{\bar{m}'}\right)_{z}\otimes\hat{\sigma}_{z}=\lambda_{\mathrm{so}}\hat{\pi}_{2}\otimes\hat{\sigma}_{z}\end{aligned} \tag{B.8}$$

The summand in Eq. (B.8) is real, but $\hat{H}_{\mathrm{SO}}$ is Hermitian meaning that

$$\left\langle n,\tau;\mu\left|\hat{H}_{\mathrm{SO}}(\tau\mathbf{K})\right|n',\tau;\mu'\right\rangle\propto\hat{\pi}_{2}.$$

Besides, Eq. (B.8) also demonstrates λ_{SO} is τ-independent.

In summary, we have

$$\left\langle n,\tau;\mu\left|\hat{H}_{0}\left(\tau\mathbf{K}\right)+\hat{H}_{\mathbf{q}}(\tau\mathbf{K})\cdot\mathbf{q}+\hat{H}_{\mathrm{SO}}(\tau\mathbf{K})\right|n',\tau;\mu'\right\rangle=$$

$$\begin{pmatrix}\varepsilon_{0}+\tau h_{x}q_{x} & \tau h_{y}q_{y}-i\lambda_{\mathrm{SO}} & 0 & 0\\ \tau h_{y}q_{y}+i\lambda_{\mathrm{SO}} & \varepsilon_{0}-\tau h_{x}q_{x} & 0 & 0\\ 0 & 0 & \varepsilon_{0}+\tau h_{x}q_{x} & \tau h_{y}q_{y}+i\lambda_{\mathrm{SO}}\\ 0 & 0 & \tau h_{y}q_{y}-i\lambda_{\mathrm{SO}} & \varepsilon_{0}-\tau h_{x}q_{x}\end{pmatrix}.$$

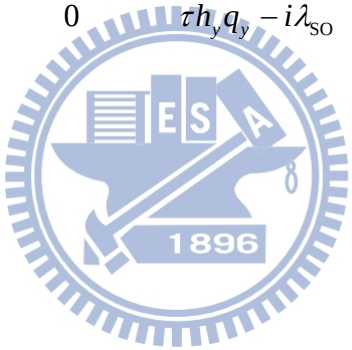

Appendix C

Band structures in a wider energy range

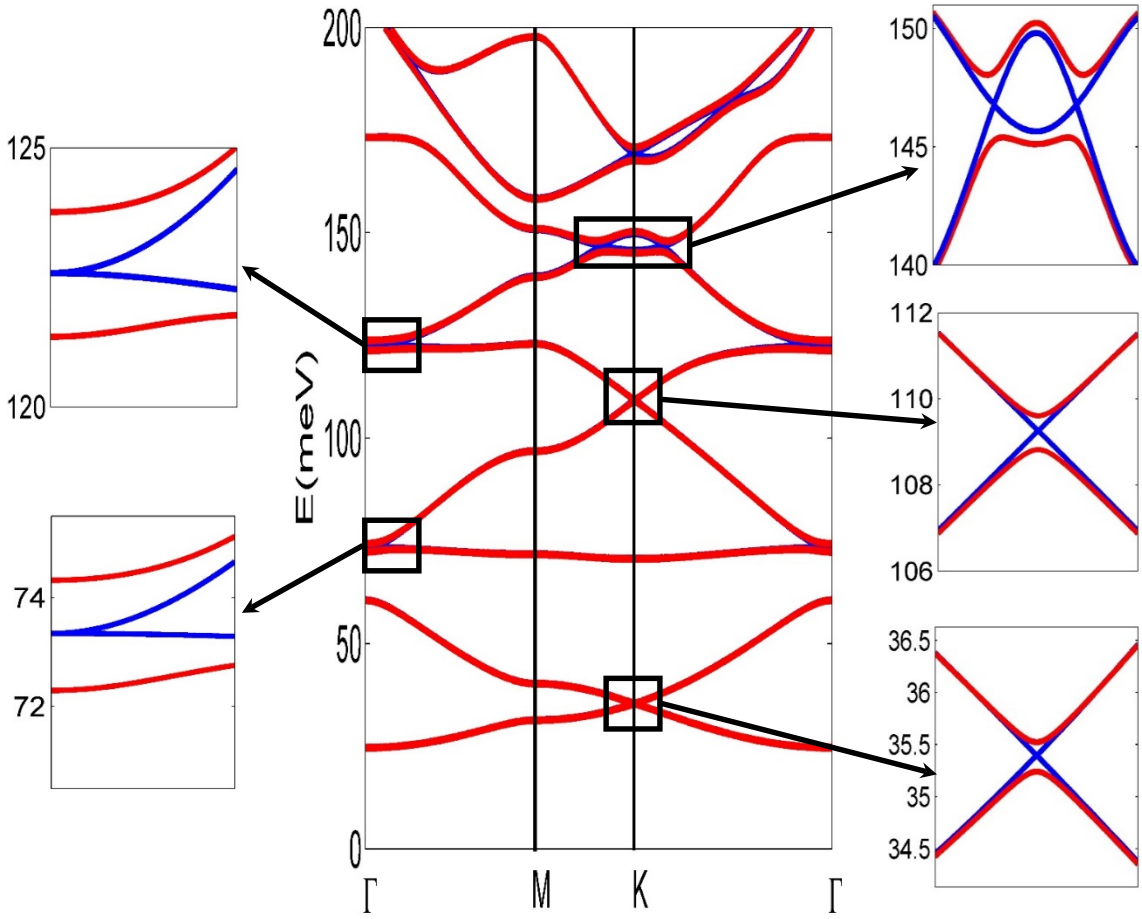

Fig. C.1: The energy band structures of 2DEG subjected to MTP lattice. The blue lines are those without SOI while the red lines are those with SOI. The parameters we employ here are $m^* = 0.023m_e$; the MTP strength $U_0 = 165$ meV with diameter, $d = 0.663a$, where $a = 40$ nm is the lattice constant. The SOI coupling constant is $\lambda = 120\text{Å}^2$.

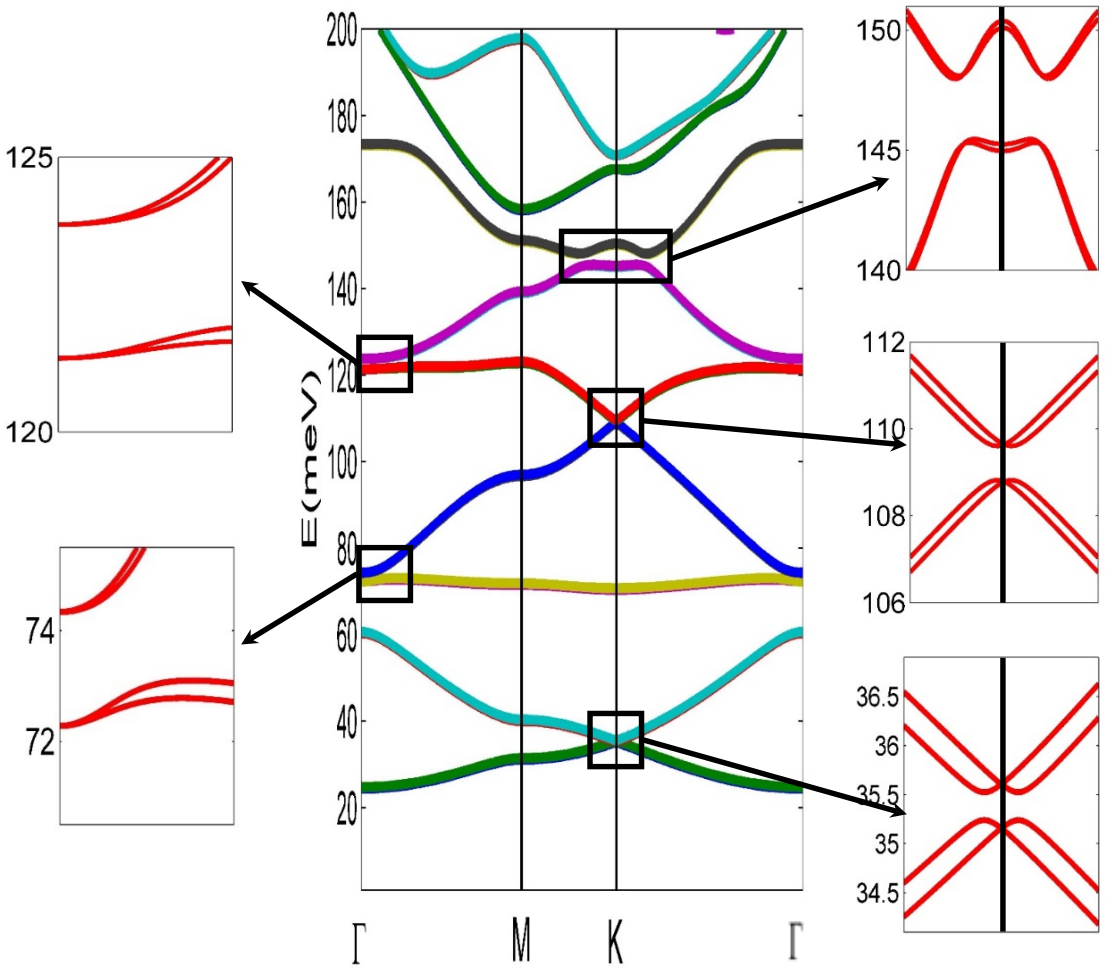

Fig. C.2: The energy band structures of 2DEG subjected to MTP with SOI and in-plane magnetic field, $\mathbf{B}_{\parallel} = 3\text{T}$. The parameters we employ here are $m^* = 0.023m_e$; the MTP strength $U_0 = 165\text{meV}$ with diameter, $d = 0.663a$, where $a = 40\ \text{nm}$ is the lattice constant. The SOI coupling constant is $\lambda = 120\text{Å}^2$.

Appendix D

An analytical discussion of the band crossing at τK

Here, we will analytical demonstrate the band touching points of the at τ**K** shown in **Fig.** D.1 is crossing rather than anti-crossing. First of all, let define the Hamiltonian be $\hat{H}_0 + \hat{H}_{\parallel} + \hat{H}_{\mathrm{SO}}$ with the unperturbed term, $\hat{H}_0 + \hat{H}_{\parallel}$ and the perturbation, $\hat{H}_{\mathrm{SO}}$. There are two degenerate points at τ**K** for the unperturbed Hamiltonian and let's denote the two pairs of degenerate states to be $\{|1,\tau;\chi_+\rangle, |2,\tau;\chi_+\rangle\}$ and $\{|1,\tau;\chi_-\rangle, |2,\tau;\chi_-\rangle\}$. Here we concentrate on the first pair states, without loss generality, and show that the perturbation, $\hat{H}_{\mathrm{SO}}$, would not remove the degeneracy between these states.

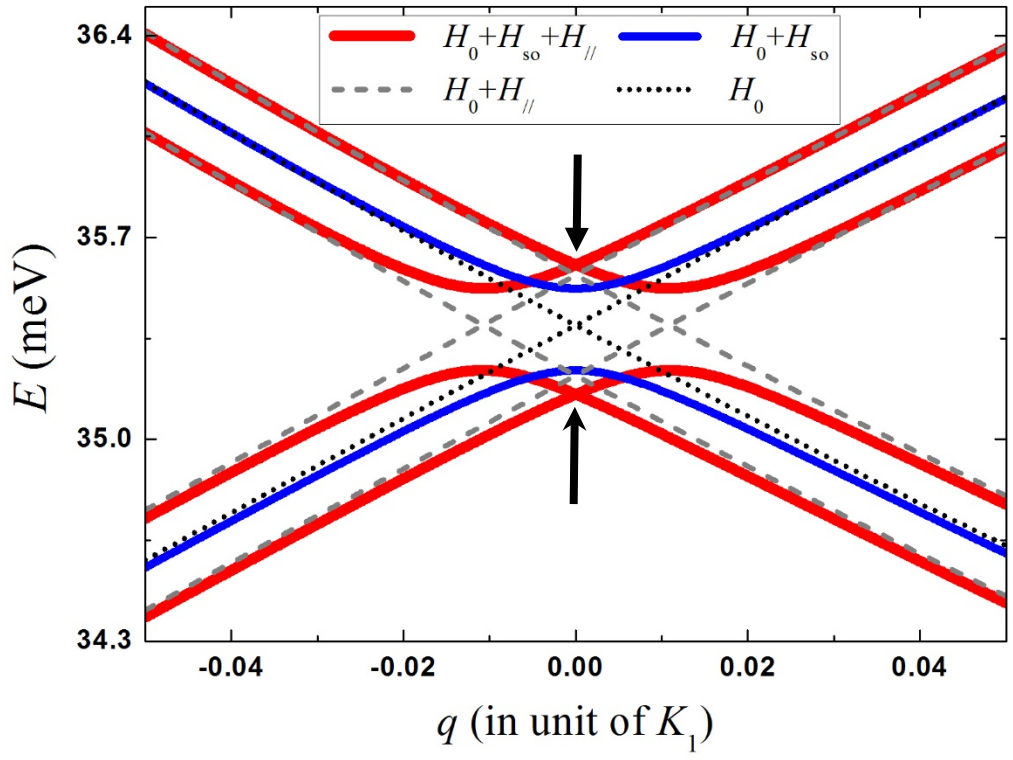

Fig. D.1: Energy dispersion with in-plane magnetic field at the lowest four bands. At K point, there are two degenerate points, indicated by the two black arrows. λ =120 Å^2 (InAs); $m^* = 0.023m_e$; $U_0 = 165$meV; $a = 40$nm; $d = 0.663a$; $B_{\mathrm{in}} = 3$(Tesla).

There are two routes to couple $|1,\tau;\chi_+\rangle$ and $|2,\tau;\chi_+\rangle$ via $\hat{H}_{\mathrm{SO}}$. The first one is from direct coupling between them, $\langle 1,\tau;\chi_+|\hat{H}_{\mathrm{SO}}|2,\tau;\chi_+\rangle$ which is zero since $\hat{H}_{\mathrm{SO}}$ flips in-plane spin. While the other one is indirect coupling,

$$\langle 1,\tau;\chi_+|\widehat{H}_{\mathrm{SO}}|n,\tau;\chi_-\rangle\langle n,\tau;\chi_-|\widehat{H}_{\mathrm{SO}}|2,\tau;\chi_+\rangle \quad \text{(D.1)}$$

with the intermediate states $|n,\tau;\chi_-\rangle$. Note that the spinor of the intermediate states must be orthogonal to those of $|1,\tau;\chi_+\rangle$ and $|2,\tau;\chi_+\rangle$. To show the matrix element product in Eq. (D.1), the parities of the states and SOI will be employed.

From the discussion in **Sec. 2.1**, the lowest two bands have different parity under the symmetry operation of $y \to -y$. However, $\widehat{H}_{\mathrm{SO}} = -\frac{\lambda}{\hbar}\hat{\boldsymbol{\sigma}}\cdot\nabla V\times\hat{\boldsymbol{p}}$ is invariant under the same symmetry operation. The parity of intermediate state, $|n,\tau;\chi_-\rangle$, must be opposite to both $|1,\tau;\chi_+\rangle$ and $|2,\tau;\chi_+\rangle$. However, the parities of $|1,\tau;\chi_+\rangle$ and $|2,\tau;\chi_+\rangle$ are already different, which means $|n,\tau;\chi_-\rangle$ cannot exist. Therefore we have proved that SOI cannot couple the degenerate states, and the band touching in Fig. E.1 is exactly crossing.

Appendix E

The values of $F_{n,\tau}(\boldsymbol{q}=0)$ and $F_{n,\tau}(\boldsymbol{q}\to\infty)$

In this appendix, we have to find the eigen-states of the effective Hamiltonian,

$$\hat{H}^{(\mathrm{eff})}(\tau\mathbf{K}+\mathbf{q}) = \varepsilon_0 + \begin{pmatrix} -\tau hq+\varepsilon_{\parallel} & -i\lambda_{\mathrm{SO}} & \gamma_{\perp}\varepsilon_{\perp} & 0 \\ +i\lambda_{\mathrm{SO}} & \tau hq-\varepsilon_{\parallel} & 0 & \gamma_{\perp}\varepsilon_{\perp} \\ \gamma_{\perp}\varepsilon_{\perp} & 0 & -\tau hq-\varepsilon_{\parallel} & -i\lambda_{\mathrm{SO}} \\ 0 & \gamma_{\perp}\varepsilon_{\perp} & +i\lambda_{\mathrm{SO}} & \tau hq+\varepsilon_{\parallel} \end{pmatrix} \quad \text{(E.1)}$$

$$= \varepsilon_0 + \begin{pmatrix} \hat{h}_1 & \gamma_{\perp}\varepsilon_{\perp}\hat{\mathbf{1}} \\ \gamma_{\perp}\varepsilon_{\perp}\hat{\mathbf{1}} & \hat{h}_2 \end{pmatrix}$$

defined in Eq. (4.7) with basis set being

$$\left\{\left|n,\tau,\mathbf{q};\chi\right\rangle \equiv \left|n,\tau,\mathbf{q}\right\rangle \otimes \left|\chi\right\rangle\right\} = \left\{\left|1,\tau,\mathbf{q};\chi_{+}\right\rangle,\left|2,\tau,\mathbf{q};\chi_{-}\right\rangle,\left|1,\tau,\mathbf{q};\chi_{-}\right\rangle,\left|2,\tau,\mathbf{q};\chi_{+}\right\rangle\right\}.$$

The $\hat{h}_1$ and $\hat{h}_2$, here, are

$$\begin{aligned} \hat{h}_1 &= -\left(\tau hq-\varepsilon_{\parallel}\right)\hat{\sigma}_z + \lambda_{\mathrm{SO}}\hat{\sigma}_y \\ \hat{h}_2 &= -\left(\tau hq+\varepsilon_{\parallel}\right)\hat{\sigma}_z + \lambda_{\mathrm{SO}}\hat{\sigma}_y \end{aligned} \quad \text{(E.2)}$$

And the eigen-value equation would be

$$\begin{pmatrix} \hat{h}_1 & \gamma_{\perp}\varepsilon_{\perp}\hat{\mathbf{1}} \\ \gamma_{\perp}\varepsilon_{\perp}\hat{\mathbf{1}} & \hat{h}_2 \end{pmatrix}\begin{pmatrix} \alpha \\ \beta \end{pmatrix} = \varepsilon\begin{pmatrix} \alpha \\ \beta \end{pmatrix}, \text{ and}$$

$$\begin{aligned} \alpha &= \gamma_{\perp}\varepsilon_{\perp}^{-1}\left(\varepsilon-\hat{h}_2\right)\beta \\ \beta &= \gamma_{\perp}\varepsilon_{\perp}^{-1}\left(\varepsilon-\hat{h}_1\right)\alpha \end{aligned} \quad , \quad \text{(E.3)}$$

which directly leads to

$$\begin{aligned} &\left\{\left(\varepsilon-\hat{h}_2\right)\left(\varepsilon-\hat{h}_1\right)-\varepsilon_{\perp}^2\right\}\alpha = 0, \text{ and} \\ &\det\left\{\left(\varepsilon-\hat{h}_2\right)\left(\varepsilon-\hat{h}_1\right)-\varepsilon_{\perp}^2\right\} \\ &= \det\left\{\varepsilon^2+\lambda_{\mathrm{SO}}^2+h^2q^2-\varepsilon_{\parallel}^2-\varepsilon_{\perp}^2+2\tau\varepsilon hq\hat{\sigma}_z-2\varepsilon\lambda_{\mathrm{SO}}\hat{\sigma}_y+2i\varepsilon_{\parallel}\lambda_{\mathrm{SO}}\sigma_x\right\}=0 \end{aligned} \quad \text{(E.4)}$$

By Eq. (E.4), we have the equation

$$\begin{aligned} &\left(\varepsilon^2+\lambda_{\mathrm{SO}}^2+h^2q^2-\varepsilon_{\parallel}^2-\varepsilon_{\perp}^2\right)^2-4\varepsilon^2h^2q^2-4\varepsilon^2\lambda_{\mathrm{SO}}^2+4\varepsilon_{\parallel}^2\lambda_{\mathrm{SO}}^2= \\ &\left(\varepsilon^2-\lambda_{\mathrm{SO}}^2-h^2q^2-\varepsilon_{\parallel}^2-\varepsilon_{\perp}^2\right)^2-4\lambda_{\mathrm{SO}}^2\varepsilon_{\perp}^2-4h^2q^2\varepsilon_{\parallel}^2-4h^2q^2\varepsilon_{\perp}^2=0 \end{aligned},$$

which determines the eigen-energies (with the labels $\eta=\pm1$ and $\xi=\pm1$) to be

Appendix E The values of $F_{n,\tau}(q=0)$ and $F_{n,\tau}(q\to\infty)$

$$\varepsilon_{\eta\xi}(\mathbf{q})=\eta\sqrt{\lambda_{\mathrm{SO}}^2+h^2q^2+\varepsilon_{\parallel}^2+\varepsilon_{\perp}^2+2\xi\sqrt{\lambda_{\mathrm{SO}}^2\varepsilon_{\perp}^2+h^2q^2\varepsilon_{\parallel}^2+h^2q^2\varepsilon_{\perp}^2}}=\eta\varepsilon_{\xi}(\mathbf{q}). \quad \text{(E.5)}$$

At $\mathbf{q}=0$,

$$\varepsilon_{\eta\xi}(\mathbf{q}=0)=\eta\sqrt{\lambda_{\mathrm{SO}}^2+\varepsilon_{\parallel}^2+\varepsilon_{\perp}^2+2\xi\lambda_{\mathrm{SO}}\varepsilon_{\perp}}=\eta\sqrt{\left(\lambda_{\mathrm{SO}}+\xi\varepsilon_{\perp}\right)^2+\varepsilon_{\parallel}^2}=\eta\varepsilon_{\xi}(0), \quad \text{(E.6)}$$

and from Eq. (E.4), we have

$$\begin{aligned}
&\left\{\varepsilon_{\eta\xi}^2+\lambda_{\mathrm{SO}}^2-\varepsilon_{\parallel}^2-\varepsilon_{\perp}^2-2\varepsilon_{\eta\xi}\lambda_{\mathrm{SO}}\hat{\sigma}_y+2i\varepsilon_{\parallel}\lambda_{\mathrm{SO}}\sigma_x\right\}\alpha_{\eta\xi}\\
&=2\lambda_{\mathrm{SO}}\left\{\lambda_{\mathrm{SO}}+\xi\varepsilon_{\perp}-\varepsilon_{\eta\xi}\hat{\sigma}_y+i\varepsilon_{\parallel}\sigma_x\right\}\alpha_{\eta\xi}\\
&=2\lambda_{\mathrm{SO}}\left\{\left(\lambda_{\mathrm{SO}}+\xi\varepsilon_{\perp}\right)\alpha_{\eta\xi}+\begin{pmatrix}0 & i\varepsilon_{\parallel}+i\varepsilon_{\eta\xi}\\ i\varepsilon_{\parallel}-i\varepsilon_{\eta\xi} & 0\end{pmatrix}\alpha_{\eta\xi}\right\} \quad \text{(E.7)}\\
&=2\lambda_{\mathrm{SO}}\left\{s\sqrt{\varepsilon_{\xi}^2-\varepsilon_{\parallel}^2}\,\alpha_{\eta\xi}+\begin{pmatrix}0 & i\eta\left\{\varepsilon_{\xi}+\eta\varepsilon_{\parallel}\right\}\\ i\eta\left\{\varepsilon_{\xi}-\eta\varepsilon_{\parallel}\right\} & 0\end{pmatrix}\alpha_{\eta\xi}\right\}=0
\end{aligned}$$

with $s=\mathrm{sgn}(\lambda_{\mathrm{SO}}+\xi\varepsilon_{\perp})$. The definition of $\varepsilon_{\eta\xi}=\eta\varepsilon_{\xi}$ in Eqs. (E.5) and (E.6), leads to the inequalities

$$\varepsilon_{\xi}+\eta\varepsilon_{\parallel}>0 \text{ and } \varepsilon_{\xi}-\eta\varepsilon_{\parallel}>0$$

cause $\varepsilon_{\xi}>\varepsilon_{\parallel}>0$. With these, it is convenient to manipulate with the square root in the following. Eq. (E.7) determines the 2×1 column vector, α,

$$\alpha_{\eta\xi}=\begin{pmatrix}A'_{\eta\xi}\\ B'_{\eta\xi}\end{pmatrix}=\begin{pmatrix}i\eta\left\{\varepsilon_{\xi}+\eta\varepsilon_{\parallel}\right\}\\ \overline{s}\sqrt{\varepsilon_{\xi}^2-\varepsilon_{\parallel}^2}\end{pmatrix}=\begin{pmatrix}i\eta\sqrt{\varepsilon_{\xi}+\eta\varepsilon_{\parallel}}\\ \overline{s}\sqrt{\varepsilon_{\xi}-\eta\varepsilon_{\parallel}}\end{pmatrix}, \quad \text{(E.8)}$$

From Eqs. (E.3) and (E.8), we have

$$\begin{aligned}
\beta_{\eta\xi}&=\gamma_{\perp}\varepsilon_{\perp}^{-1}\left(\varepsilon_{\eta\xi}-\hat{h}_1\right)\alpha_{\eta\xi}=\gamma_{\perp}\varepsilon_{\perp}^{-1}\begin{pmatrix}\varepsilon_{\eta\xi}-\varepsilon_{\parallel} & +i\lambda_{\mathrm{SO}}\\ -i\lambda_{\mathrm{SO}} & \varepsilon_{\eta\xi}+\varepsilon_{\parallel}\end{pmatrix}\begin{pmatrix}A'_{\eta\xi}\\ B'_{\eta\xi}\end{pmatrix}\\
&=\gamma_{\perp}\varepsilon_{\perp}^{-1}\begin{pmatrix}\eta\left\{\varepsilon_{\xi}-\eta\varepsilon_{\parallel}\right\}A'_{\eta\xi}+i\lambda_{\mathrm{SO}}B'_{\eta\xi}\\ \eta\left\{\varepsilon_{\xi}+\eta\varepsilon_{\parallel}\right\}B'_{\eta\xi}-i\lambda_{\mathrm{SO}}A'_{\eta\xi}\end{pmatrix}
\end{aligned} \quad \text{(E.9)}$$

The normalization constant determined from Eqs. (E.8) and (E.9) is

$$\begin{aligned}
N_{\eta\xi}^2&=\left|A'_{\eta\xi}\right|^2+\left|B'_{\eta\xi}\right|^2\\
&+\varepsilon_{\perp}^{-2}\left|\eta\left\{\varepsilon_{\xi}-\eta\varepsilon_{\parallel}\right\}A'_{\eta\xi}+i\lambda_{\mathrm{SO}}B'_{\eta\xi}\right|^2+\varepsilon_{\perp}^{-2}\left|\eta\left\{\varepsilon_{\xi}+\eta\varepsilon_{\parallel}\right\}B'_{\eta\xi}-i\lambda_{\mathrm{SO}}A'_{\eta\xi}\right|^2\\
&=2\varepsilon_{\xi}+\tfrac{1}{\varepsilon_{\perp}^2}\left\{\left(\varepsilon_{\xi}-\eta\varepsilon_{\parallel}\right)\left(\varepsilon_{\xi}^2-\varepsilon_{\parallel}^2\right)+\lambda_{\mathrm{SO}}^2\left(\varepsilon_{\xi}-\eta\varepsilon_{\parallel}\right)+2\overline{s}\lambda_{\mathrm{SO}}\left(\varepsilon_{\xi}-\eta\varepsilon_{\parallel}\right)\sqrt{\varepsilon_{\xi}^2-\varepsilon_{\parallel}^2}\right\}\\
&\quad+\tfrac{1}{\varepsilon_{\perp}^2}\left\{\left(\varepsilon_{\xi}+\eta\varepsilon_{\parallel}\right)\left(\varepsilon_{\xi}^2-\varepsilon_{\parallel}^2\right)+\lambda_{\mathrm{SO}}^2\left(\varepsilon_{\xi}+\eta\varepsilon_{\parallel}\right)+2\overline{s}\lambda_{\mathrm{SO}}\left(\varepsilon_{\xi}+\eta\varepsilon_{\parallel}\right)\sqrt{\varepsilon_{\xi}^2-\varepsilon_{\parallel}^2}\right\}\\
&=2\varepsilon_{\xi}+\tfrac{1}{\varepsilon_{\perp}^2}2\varepsilon_{\xi}\left\{\overline{s}\sqrt{\varepsilon_{\xi}^2-\varepsilon_{\parallel}^2}+\lambda_{\mathrm{SO}}\right\}^2=2\varepsilon_{\xi}+\tfrac{1}{\varepsilon_{\perp}^2}2\varepsilon_{\xi}\left\{\lambda_{\mathrm{SO}}-\lambda_{\mathrm{SO}}-\xi\varepsilon_{\perp}\right\}^2=4\varepsilon_{\xi}
\end{aligned}$$

Appendix E The values of $F_{n,\tau}(\boldsymbol{q}=0)$ and $F_{n,\tau}(\boldsymbol{q}\to\infty)$

The above equation has utilized the fact that $s=\mathrm{sgn}(\lambda_{\mathrm{SO}}+\xi\varepsilon_{\perp})$. Therefore,

$$
\begin{aligned}
F_{\eta\xi,\tau}(0)=F_{\eta\xi,\bar{\tau}}(0)&=\left[D_{n,\tau}^{*}A_{n,\tau}-A_{n,\tau}^{*}D_{n,\tau}+B_{n,\tau}^{*}C_{n,\tau}-C_{n,\tau}^{*}B_{n,\tau}\right]_{q=0}\\
&=N_{\eta\xi}^{-2}\frac{\gamma_{\perp}}{\varepsilon_{\perp}}\left\{\begin{array}{l}+\left[\eta\left\{\varepsilon_{\xi}+\eta\varepsilon_{\parallel}\right\}B'_{\eta\xi}-i\lambda_{\mathrm{SO}}A'_{\eta\xi}\right]^{*}\left[A'_{\eta\xi}\right]\\-\left[A'_{\eta\xi}\right]^{*}\left[\eta\left\{\varepsilon_{\xi}+\eta\varepsilon_{\parallel}\right\}B'_{\eta\xi}-i\lambda_{\mathrm{SO}}A'_{\eta\xi}\right]\\+\left[\eta\left\{\varepsilon_{\xi}-\eta\varepsilon_{\parallel}\right\}A'_{\eta\xi}+i\lambda_{\mathrm{SO}}B'_{\eta\xi}\right]\left[B'_{\eta\xi}\right]^{*}\\-\left[B'_{\eta\xi}\right]\left[\eta\left\{\varepsilon_{\xi}-\eta\varepsilon_{\parallel}\right\}A'_{\eta\xi}+i\lambda_{\mathrm{SO}}B'_{\eta\xi}\right]^{*}\end{array}\right\}\\
&=N_{\eta\xi}^{-2}\frac{\gamma_{\perp}}{\varepsilon_{\perp}}\left\{2i\lambda_{\mathrm{SO}}\left(\left|A'_{\eta\xi}\right|^{2}+\left|B'_{\eta\xi}\right|^{2}\right)+4i\eta\varepsilon_{\xi}\,\mathrm{Im}\left(A'_{\eta\xi}B'^{*}_{\eta\xi}\right)\right\}\\
&=\frac{4i\lambda_{\mathrm{SO}}\varepsilon_{\xi}+4i\varepsilon_{\xi}\bar{s}\sqrt{\varepsilon_{\xi}^{2}-\varepsilon_{\parallel}^{2}}}{4\varepsilon_{\xi}}=i\left(\lambda_{\mathrm{SO}}+\bar{s}\sqrt{\varepsilon_{\xi}^{2}-\varepsilon_{\parallel}^{2}}\right)\\
&=i\frac{\lambda_{\mathrm{SO}}-\left(\lambda_{\mathrm{SO}}+\xi\varepsilon_{\perp}\right)}{\gamma_{\perp}\varepsilon_{\perp}}\\
&=-i\xi\gamma_{\perp}
\end{aligned}
\tag{E.9}
$$

On the other hand, from Eq. (E.1), as $\mathbf{q}\to\infty$, the effective Hamiltonian becomes

$$
\left[\hat{H}^{(\mathrm{eff})}(\tau\mathbf{K}+\mathbf{q})\right]_{\mathbf{q}\to\infty}=\varepsilon_{0}+\begin{pmatrix}-\tau hq & 0 & \gamma_{\perp}\varepsilon_{\perp} & 0\\ 0 & \tau hq & 0 & \gamma_{\perp}\varepsilon_{\perp}\\ \gamma_{\perp}\varepsilon_{\perp} & 0 & -\tau hq & 0\\ 0 & \gamma_{\perp}\varepsilon_{\perp} & 0 & \tau hq\end{pmatrix}. \tag{E.10}
$$

Note that in Eq. (E.10), $\gamma_{\perp}\varepsilon_{\perp}$ is kept as $\mathbf{q}\to\infty$ since the out-of-plane field, $\mathbf{B}_{\perp}$, couples the degenerate states $|1,\tau;\chi_{\pm}\rangle$ (with energy $\varepsilon_{0}-\tau hq$) and $|2,\tau;\chi_{\pm}\rangle$ (with energy $\varepsilon_{0}+\tau hq$). Therefore, the eigen-states are

$$
\begin{aligned}
&\cos\tfrac{\theta}{2}|1,\tau;\chi_{+}\rangle+\sin\tfrac{\theta}{2}|1,\tau;\chi_{-}\rangle,\\
&\sin\tfrac{\theta}{2}|1,\tau;\chi_{+}\rangle-\cos\tfrac{\theta}{2}|1,\tau;\chi_{-}\rangle,\\
&\cos\tfrac{\theta}{2}|2,\tau;\chi_{+}\rangle+\sin\tfrac{\theta}{2}|2,\tau;\chi_{-}\rangle,\ \text{and}\\
&\sin\tfrac{\theta}{2}|2,\tau;\chi_{+}\rangle-\cos\tfrac{\theta}{2}|2,\tau;\chi_{-}\rangle,
\end{aligned}
\tag{E.11}
$$

with energy $\varepsilon_{0}-\tau hq\pm\gamma_{\perp}\varepsilon_{\perp}$, and $\varepsilon_{0}+\tau hq\pm\gamma_{\perp}\varepsilon_{\perp}$, sequentially. Eq. (E.11) directly results in null of $F_{n,\tau}(\boldsymbol{q}\to\infty)$ because one of $A_{\eta\xi}$ and $D_{\eta\xi}$ must be zero and so does $B_{\eta\xi}$ and $C_{\eta\xi}$. In conclusion, we have

$$
\begin{aligned}
F_{\eta\xi,\tau}(q=0)&=-i\xi\gamma_{\perp}\\
F_{\eta\xi,\tau}(q\to\infty)&=0
\end{aligned}
$$

which will be utilized in the calculation of Chern number in **Sec.** 4.3.

Bibliography

[1] D. J. Thouless, M. Kohmoto, M. P. Nightingale, and M. den Nijs, Phys. Rev. Lett. 49, 405 (1982)

[2] K. v. Klitzing, G. Dorda, and M. Pepper, Phys. Rev. Lett. 45, 494 (1980)

[3] R. Laughlin, Phys. Rev. B 23,5632 (1981)

[4] C.L. Kane and E.J. Mele, Phys. Rev. Lett. 95,166605 (2005)

[5] F.D.M. Haldane, Phys. Rev. Lett. 61,2015 (1988)

[6] B.A. Bernevig, T.L. Hughes and S.C. Zhang, Science 314, 1757 (2006)

[7] Markus Konig, Steffen Wiedmann, Christoph Brune, Andreas Roth, Hartmut Buhmann, Laurens W. Molenkamp, Xiao-Liang Qi, and Shou-Cheng Zhang, Published online (2007); 10.1126/science.1148047

[8] C.L. Kane and E.J. Mele, Phys. Rev. Lett. 95, 146802 (2005)

[9] *Topics in advanced quantum mechanics*, Barry R. Holstein (Addison Wesley).

[10] Hans-Andreas Engel, Bertrand I. Halperin, and Emmanuel I. Rashba, Phys. Rev. Lett. 95, 166605 (2005)

[11] *Spin-Orbit Coupling in Two-Dimensional Electron and Hole systems*, Roland Winkler (Springer, 2003).

[12] C.L. Kane and E.J. Mele, Phys. Rev. Lett. 95, 226801 (2005)

[13] A. H. Castro Neto, F. Guinea, N. M. R. Peres, K. S. Novoselov, A. K. Geim, Rev. Mod. Phys. 81, 109 (2009)

[14] C.H. Park and S. G. Louie, Nano Lett.9, 1793 (2009)

[15] W. L. Su, 2010, *Effects spin-orbit interaction on a nano-patterned two-dimensional electron gas*, Master dissertation, National Chiao Tung University, Department of Electrophysics.

[16] A. H. Castro Neto, F. Guinea, N. M. R. Peres, K. S. Novoselov, A. K. Geim, Rev. Mod. Phys. 81, 109 (2009).